SGP-TR-174

Estimating Water Saturation at The Geysers Based on Historical Pressure and Temperature Production Data

Jericho L.P. Reyes

June 2003

Financial support was provided through the
Stanford Geothermal Program under
California Energy Commission PIER grant PIR-00-004,
and by the Department of Petroleum Engineering,
Stanford University

Stanford Geothermal Program
Interdisciplinary Research in
Engineering and Earth Sciences
STANFORD UNIVERSITY
Stanford, California

Abstract

Available historical data from 503 wells at The Geysers geothermal field were analyzed to estimate in-situ water saturation using zero-dimensional models of the reservoir. The pressure and temperature performance data of most of the wells demonstrate "dry-out" due to the formation of superheated steam. The in-situ water saturation of the reservoir can be inferred by using zero-dimensional models derived from mass and energy conservation equations. Techniques to identify the initial reservoir temperature and the dry-out temperature were developed and used in the saturation calculations. Effects of reinjection of The Geysers were analyzed and compared to models of depleted reservoirs. Regional trends of the saturation values plotted in the Cartesian plane were also investigated.

Acknowledgments

This work was funded by a PIER Grant by the California Energy Commission. We are also grateful for the assistance of the California Division of Oil, Gas and Geothermal Resources and Calpine Corporation in obtaining field data.

The author would also like to thank the members of the Stanford Geothermal Program, namely Roland Horne, Kewen Li and Allan Chen, for their invaluable help and support.

Contents

List of Tables

List of Figures

Chapter 1

1. Introduction

The Geysers geothermal field in Northern California is the largest producing vapor-dominated field in the world. The exploitation of the geothermal reservoir entails the extraction of thermal energy, which is then used to generate electricity. Accurate knowledge of the parameters involved in this recovery process is of substantial economic value in making most effective use of the resource.

Exploitation of a geothermal field is dependent on the quantity of heat available in the reservoir and on how long it can be extracted (Bowen, 1989). Recovery of energy from a geothermal reservoir requires that mass be withdrawn from it. Once a reservoir has reached its maximum exploitative capacity, no more fluid can be extracted unless additional recharge liquid is injected into the reservoir artificially. Understanding when fluid will be exhausted and how much remains at any moment are important to predicting the ultimate recovery of the resource.

The basic components of a vapor-dominated geothermal reservoir are its reserves of steam and immobile water. Under exploitation the vapor-dominated field can be locally depleted of water to form a dry or superheated zone. There is a recharge of steam from boiling of the immobile water. Even though the steam is the principal recovery fluid, by mass the immobile water represents a much larger component of the reservoir fluid than the steam. Hence quantifying the immobile water in the reservoir is of particular importance.

Knowledge of the immobile and in-situ water saturation will also provide better understanding of the fluid storage capacities of geothermal rocks, as this is valuable in estimating the performance of a geothermal reservoir and its capacity for further exploitation.

Past projects have relied on numerical simulation to infer field conditions. Similar techniques have also been used to infer flow and saturation properties from experimental measurements. Belen and Horne (2000) used numerical simulation to verify values of in-situ and immobile water saturations calculated from zero-dimensional models based on those described in Grant, Donaldson and Bixley (1982). The principal objective of this study was to use Belen's model to match field data from The Geysers and thereby estimate the immobile water saturation.

These studies used numerical simulation to verify and extend present field measurements or experimental values. Numerical simulation provides a means to predict and visualize

the performance of a certain system under known parameters (Pruess, 1991). Simulating a geothermal reservoir's behavior during exploitation allows us to infer reservoir parameters, forecast future performance and design optimal development strategy.

Chapter 2

2. Estimation of In-situ Saturation using Production Data

2.1. Geysers Database

The Geysers Geothermal Field is located in Northern California about 130 km north of San Francisco. Since 1987, The Geysers has experienced a decline in steam pressure (Barker and Pingol, 1997). Recovering some of the reduced reservoir capacity has been achieved by injecting water into parts of The Geysers reservoir to recover additional heat.

The Geysers production database was made available by the California Division of Oil, Gas and Geothermal Resources. The Geysers database, which contains temperature and pressure values for 502 wells around The Geysers field area, also contains information on the history and overall structure of the wells. As an illustrative example, this report will describe two wells from The Geysers database, namely McKinley 1 and Thorne 1, located in the Lake and Sonoma Counties. McKinley 1, a redrilled active producer well owned by the Calpine Geysers Company, had a depth of 2219.18 feet. Thorne 1, also an active producer well, has a depth of 6842 feet.

The pressure-temperature profiles of the wells, gathered over a period of 20 years, are plotted against the steam saturation curve and shown in Figure 2-1 and Figure 2-2.

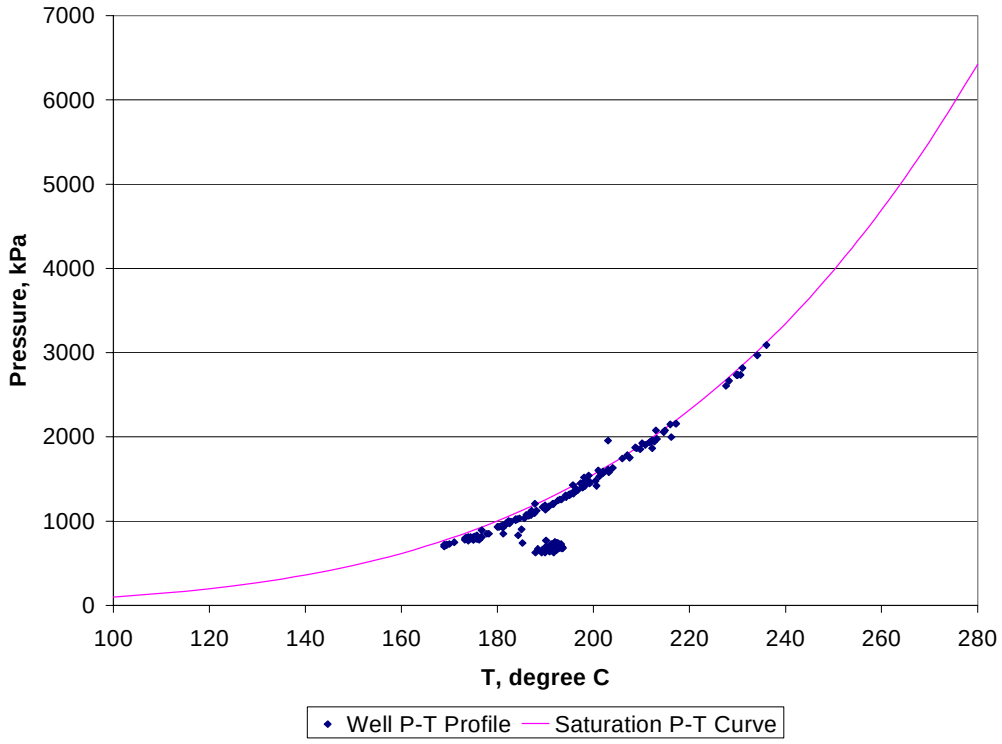

Figure 2-1: Pressure-temperature profile of the McKinley 1 well.

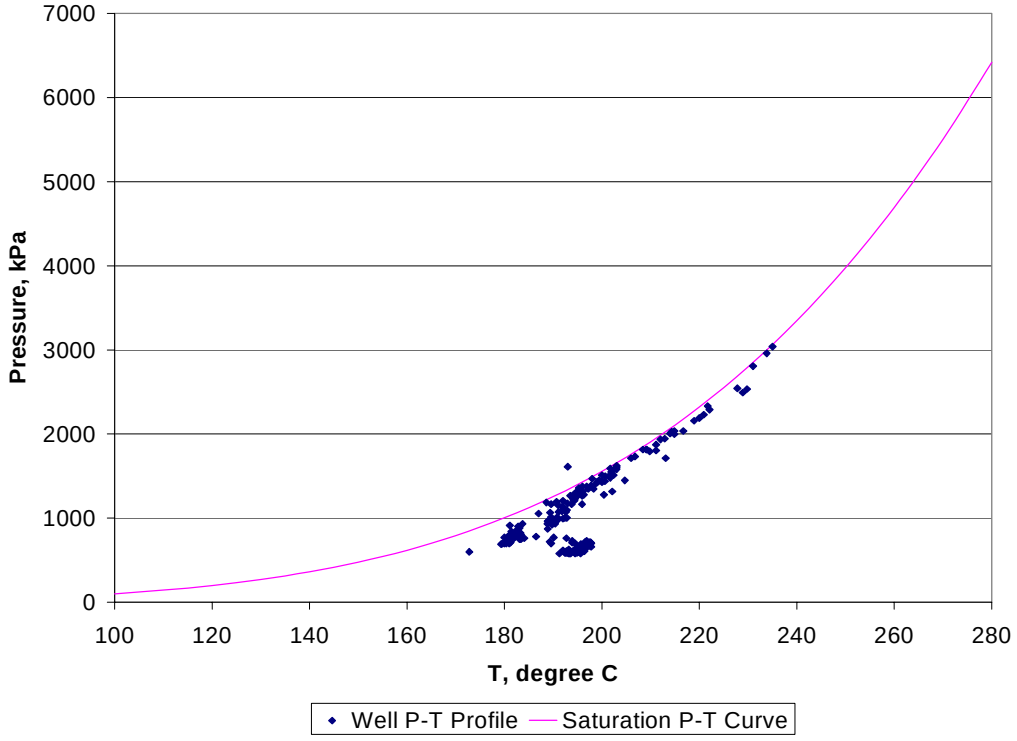

Figure 2-2: Pressure-temperature profile of the Thorne 1 well.

The well pressure-temperature profiles suggest a clear relationship with the saturation pressure temperature curve of water. A noticeable deviation is the formation of a cluster at the lower pressure values under the saturation curve. The formation of this "elbow" in the pressure-temperature profile, in which the pressure values are lower than the saturated values for a certain temperature, can be attributed to the point in the exploitation history at which the immobile saturation of the water in the reservoir has been boiled away. The immobile saturation of the water is liquid that cannot flow in the reservoir, and hence represents an "invisible" phase. Nonetheless, the immobile water will become steam during exploitation, due to boiling, and hence is a very important source of energy.

To better understand when this phenomenon happens, we plotted the histories of the well over the same 20-year span. The result is shown in Figure 2-3 and Figure 2-4.

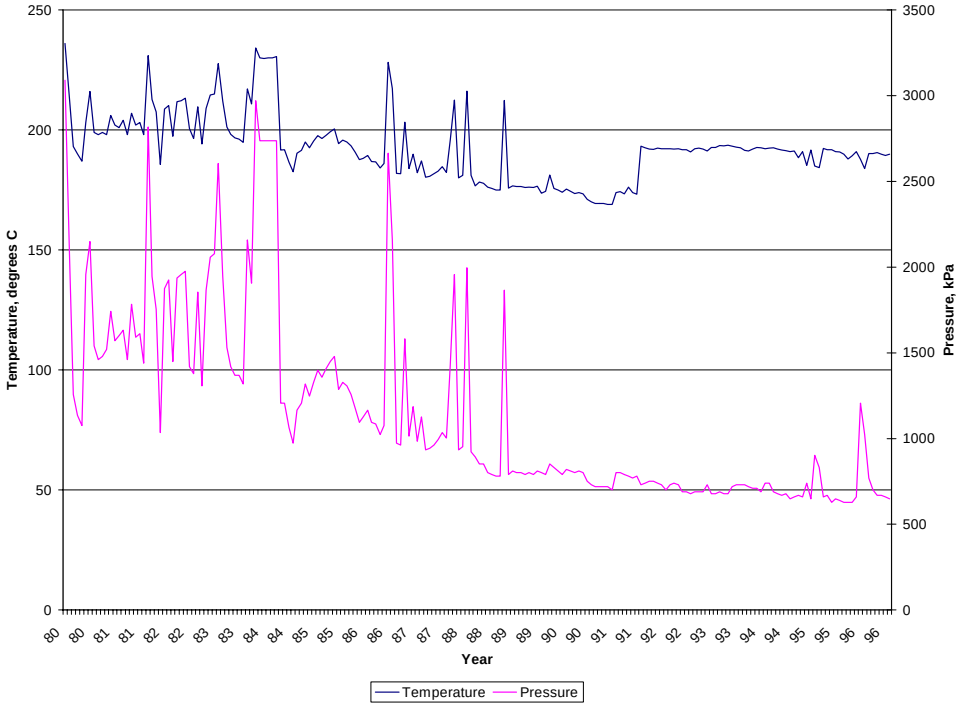

Figure 2-3: Temperature and pressure history for the McKinley 1 well.

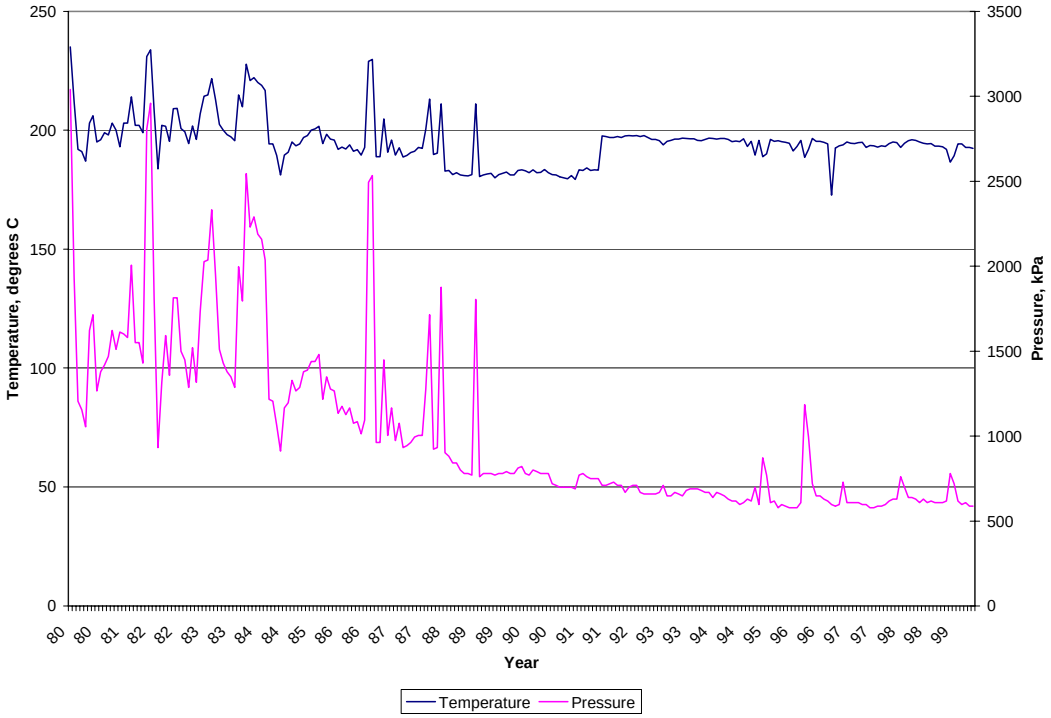

Figure 2-4: Temperature and pressure history for the Thorne 1 well.

It can be seen in the left side of Figure 2-3 that the temperature fluctuates in the same manner as the pressure, or when the pressure goes up, the temperature goes up too. This trend is noticed from years 1980 to 1991. After a brief leveling off, the trend goes the opposite way, or when the temperature goes down, the pressure goes up and vice versa. Whether or not these phenomena are attributable to the point in the reservoir exploitation where the immobile water saturation has boiled away is examined in the following sections. Similar trends can be seen in Figure 2-4.

2.2. Previous Results in Simulation and Modeling

In order to generate similar curves for temperature and pressure of a producer well under exploitation, we need to produce numerical models to simulate the geothermal reservoir under exploitation. This will allow us to investigate whether the elbow in the pressure-temperature profile is indeed because the reservoir has boiled away the immobile water saturation.

In 2000, Belen developed a two-phase radial reservoir model to determine the end-point saturation of steam and liquid water relative permeability curves by inference from pressure, temperature and saturation data. The objective of the study was to determine the end-points based on both zero-dimensional models and from numerical simulation.

2.2.1. Zero-Dimensional Model

Geothermal reservoirs under exploitation can be modeled using zero-dimensional models derived from material and energy conservation equations and Darcy's Law. Using the characteristics of vapor-dominated reservoirs, which primarily is the classification of The Geysers, where the mobile phase is steam, Darcy's Law describes the steam flow.

$$\phi \frac{\partial}{\partial t}\{s\rho_w + (1-s)\rho_s\} = -\nabla \cdot (\vec{u}_s \rho_s) \tag{2-1}$$

$$\frac{\partial}{\partial t}\{(1-\phi)\rho_r c_r T + \phi(1-s)\rho_s h_s\} = -\nabla \cdot (\vec{u}\rho_s h_s) \tag{2-2}$$

$$\vec{u} = \frac{k k_{rs}}{\mu_s} \nabla p \tag{2-3}$$

The enthalpy of saturated steam is nearly constant with temperature under reservoir conditions. This allows the simplification of the energy conservation equation relating pressure and saturation.

$$(1-\phi)\rho_r C_r T + \phi s \rho_w (h_w - h_s) = \text{constant} \tag{2-4}$$

Belen (2000) derived a zero-dimensional model that allows us to calculate the in-situ water saturation using rock and fluid properties,

$$s_o = \frac{(1-\phi)}{\phi} \frac{\rho_r c_r (T_o - T_d)}{\rho_w (h_s - h_w)\big|_{T_o}} \tag{2-5}$$

where T_o is the initial reservoir temperature and T_d is the dry-out temperature.

2.2.2. TOUGH2 Two-Phase Radial Flow Model

A two-phase radial flow was modeled using the numerical simulator TOUGH2 (Pruess, 1991). A cylindrical model was used in the simulation runs. A single well was placed in the middle of the reservoir. Table 2-1 summarizes the parameters used for the runs.

Table 2-1: Reservoir properties used in the simulation.

Porosity	5%
Permeability	1×10^{-13} m^2
Rock Density	2600 kg / m^3
Rock Specific Heat	485 J / kg ºC
Reservoir Radius	1000 m
Reservoir Thickness	10 m
Initial Reservoir Temperature	280 ºC

The model consisted of 100 grid blocks, with grid size increasing logarithmically from the center to the boundary of the reservoir.

Figure 2-5 compares the production enthalpies simulated by TOUGH2 with those predicted by the zero-dimensional model with in-situ water saturation of 0.3. There is good agreement between the simulator and the model results. Figure 2-6 shows another vapor-dominated case, this time with a higher in-situ saturation to 0.3.

In these two cases, the zero-dimensional model simulated reservoir temperatures satisfactorily in comparison to the values computed with TOUGH2. Therefore, it is reasonable to use the zero-dimensional model to analyze the data taken from actual wells in The Geysers geothermal field. It should be noted that the ability of a volume-averaged model to replicate the fully dimensional result justifies the application to The Geysers, which is admittedly a heteregoneous and fractured reservoir. The pressure-temperature history data from the Geysers is analyzed over long periods (e.g. 20 years), during which time the bulk behavior is not expected to be governed by fractures and heterogeneities.

The study concluded that both in-situ and immobile water saturations could be inferred from field measurements using simple zero-dimensional models and TOUGH2 two-phase radial flow simulation results.

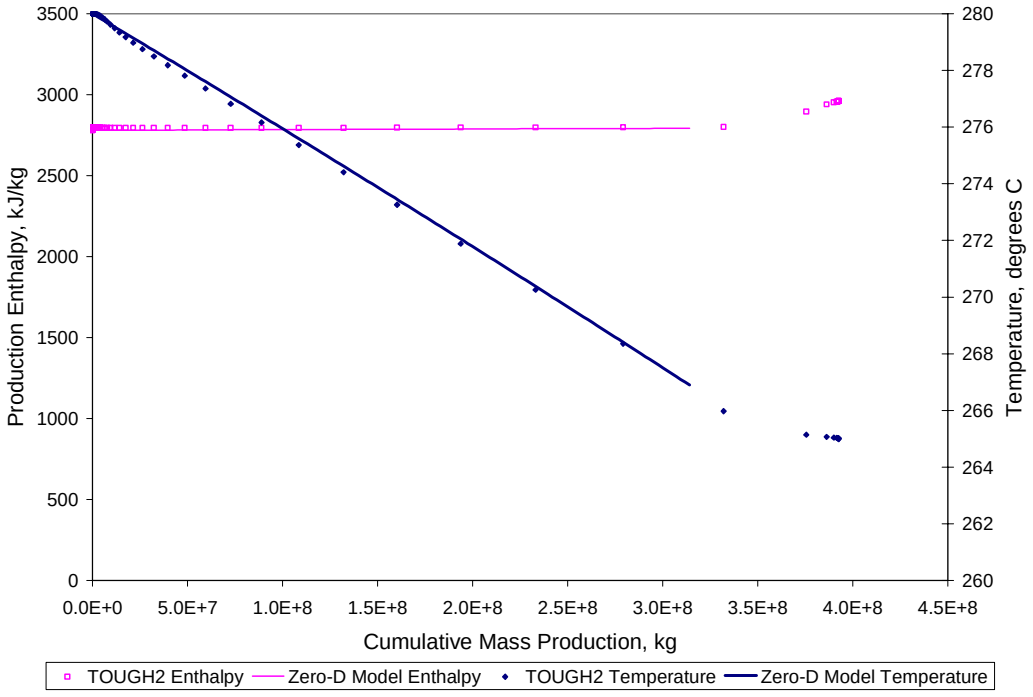

Figure 2-5: Production enthalpy and reservoir temperature profiles: initial water saturation = 0.3, irreducible water saturation = 0.3 (Belen, 2000).

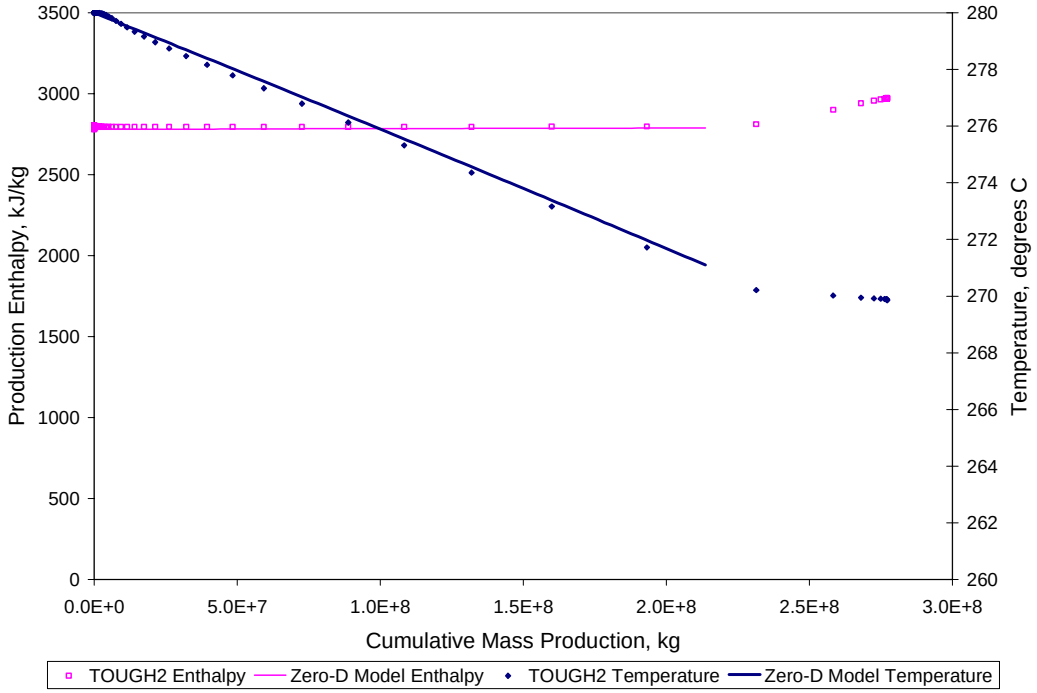

Figure 2-6: Production enthalpy and reservoir temperature profiles: initial water saturation = 0.2, irreducible water saturation = 0.2 (Belen, 2000).

2.3. Numerical Simulation of Pressure-Temperature Profiles

Using the two-phase radial model developed by Belen (2000), and using the parameters given in Table 2-1, TOUGH2 simulations were made and pressure-temperature profiles were plotted. These plots are shown in Figure 2-7 and Figure 2-8, with irreducible water saturation taken as 0.3 and 0.2 respectively.

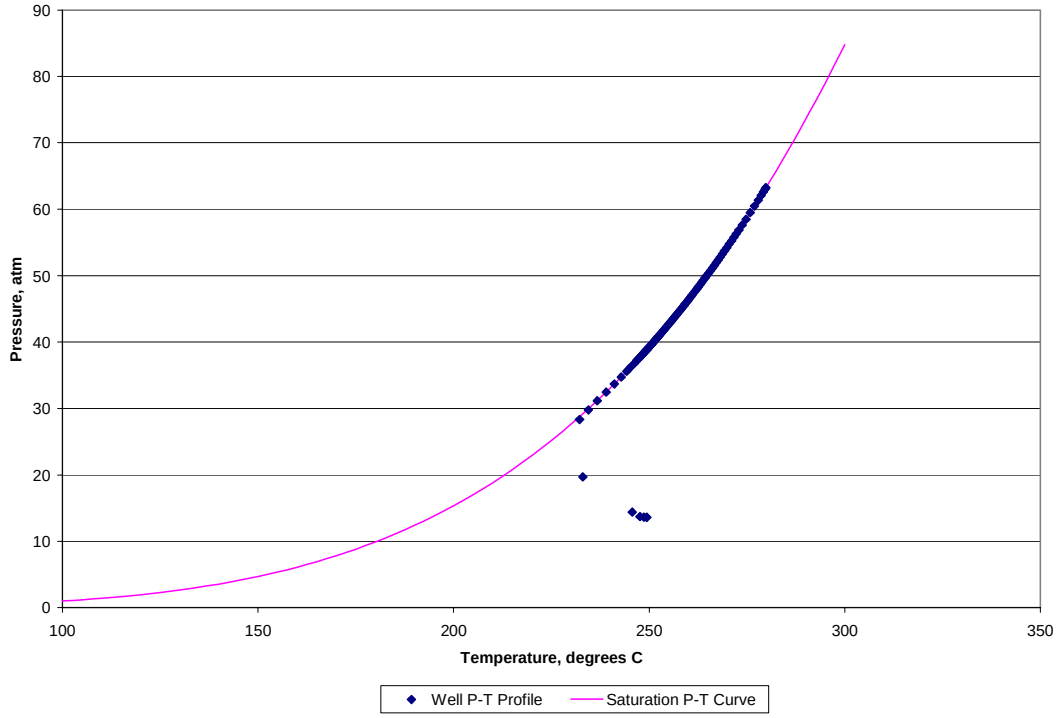

Figure 2-7: Pressure-temperature profile of the TOUGH2 simulated model, irreducible water saturation = 0.3.

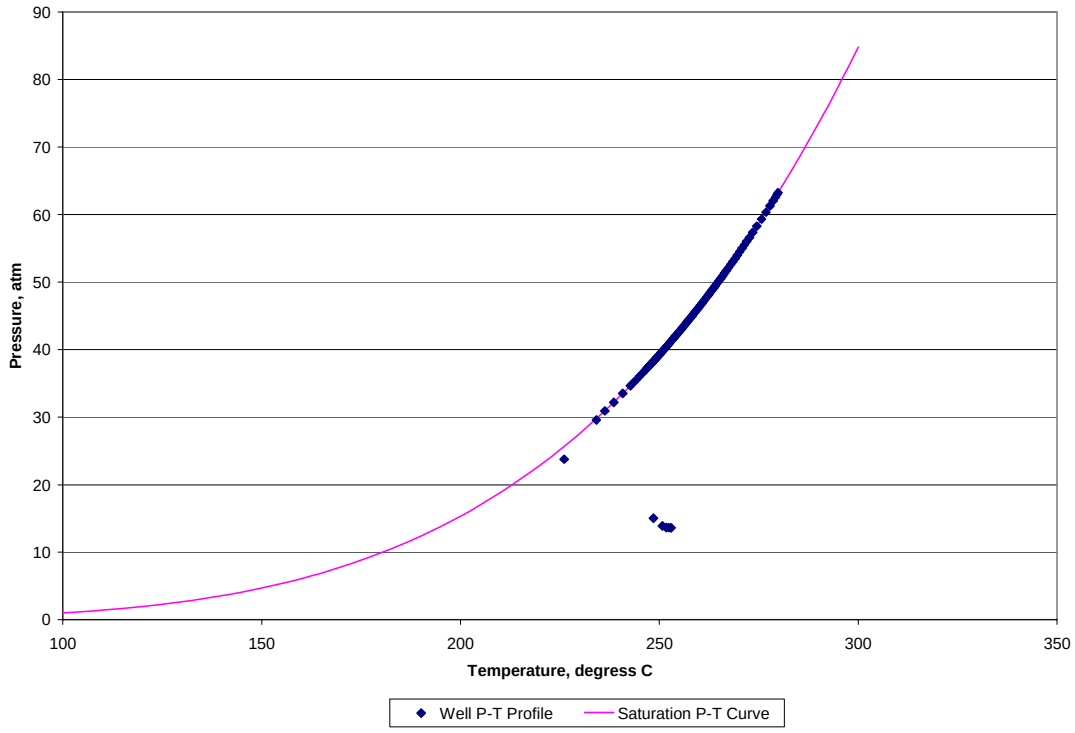

Figure 2-8: Pressure-temperature profile of the TOUGH2 simulated model, irreducible water saturation = 0.2.

The simulated values follow the saturation curve, with the appearance of an elbow, similar to the data seen in wells McKinley 1 and Thorne 1. The simulation shows that when the reservoir reaches zero saturation, a lowering of pressure is observed as the well zone becomes superheated. Pressure values decrease and deviate from the saturation curve.

The history of the exploitation of the simulated reservoir is plotted in Figure 2-9 and Figure 2-10 for 0.3 and 0.2 values of in-situ water saturation, respectively, to better understand at what point this elbow occurs and if it is comparable with the actual well histories plotted in Figure 2-3 and 2-4.

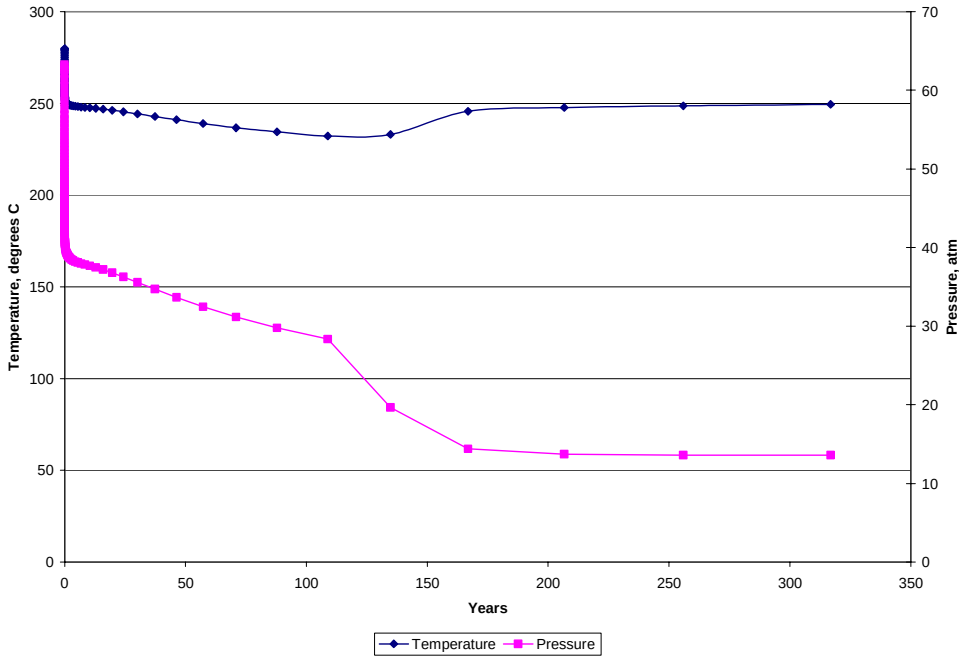

Figure 2-9: Temperature and pressure history for the TOUGH2 simulated model, irreducible water saturation = 0.3.

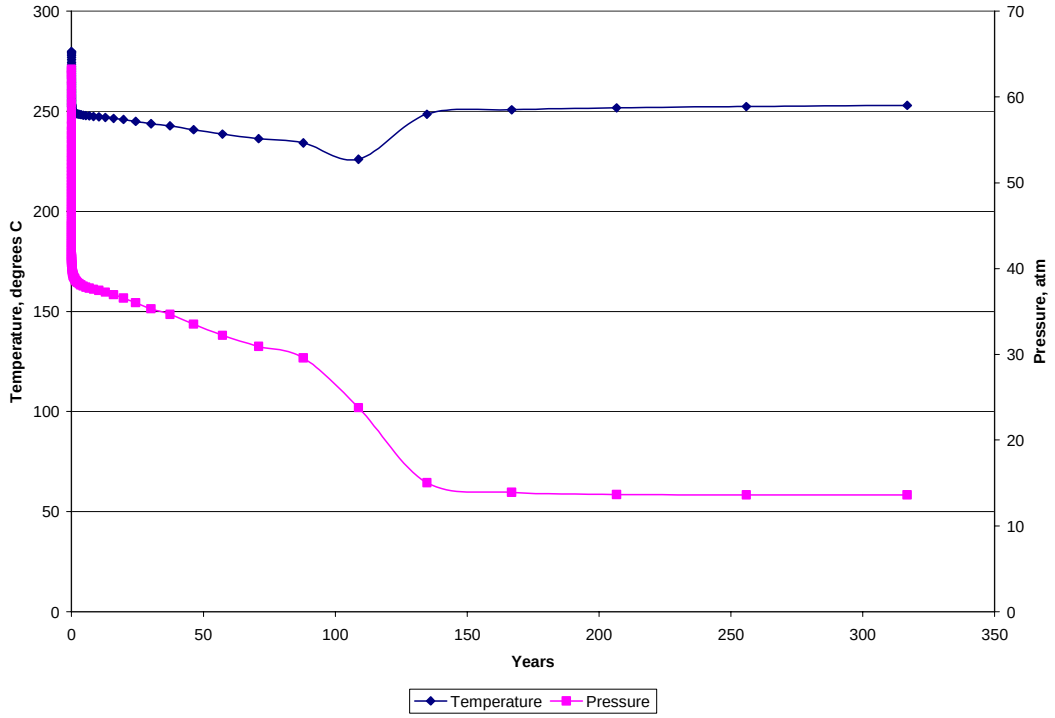

Figure 2-10: Temperature and pressure history for the TOUGH2 simulated model, irreducible water saturation = 0.2.

For both graphs, the temperature and pressure histories from 0 to 100 years are in direct relationship, that is, when pressure decreases, the temperature also decreases. After that, however, the opposite relationship exists, or as the temperature goes up, the pressure goes down. The point at which the behavior changes corresponds to the formation of the elbow in Figure 2-7 and Figure 2-8, and is indicative of the reservoir reaching zero water saturation. This confirms the proposed explanation of the behavior of the McKinley 1 and Thorne 1 wells, which showed a similar phenomenon.

To verify these results, we calculated the in-situ water saturation for the simulation run using Equation 2-5. From the equation, it is seen that two temperatures are needed for the calculation of s_o. The initial reservoir temperature, T_o, is used to evaluate the fluid properties ρ_w, h_s and h_w. The dry-out temperature, T_d, is determined to be the temperature just before the well reaches s_o. These two temperatures are indicated in Figure 2-11 for the $s_o = 0.3$ run.

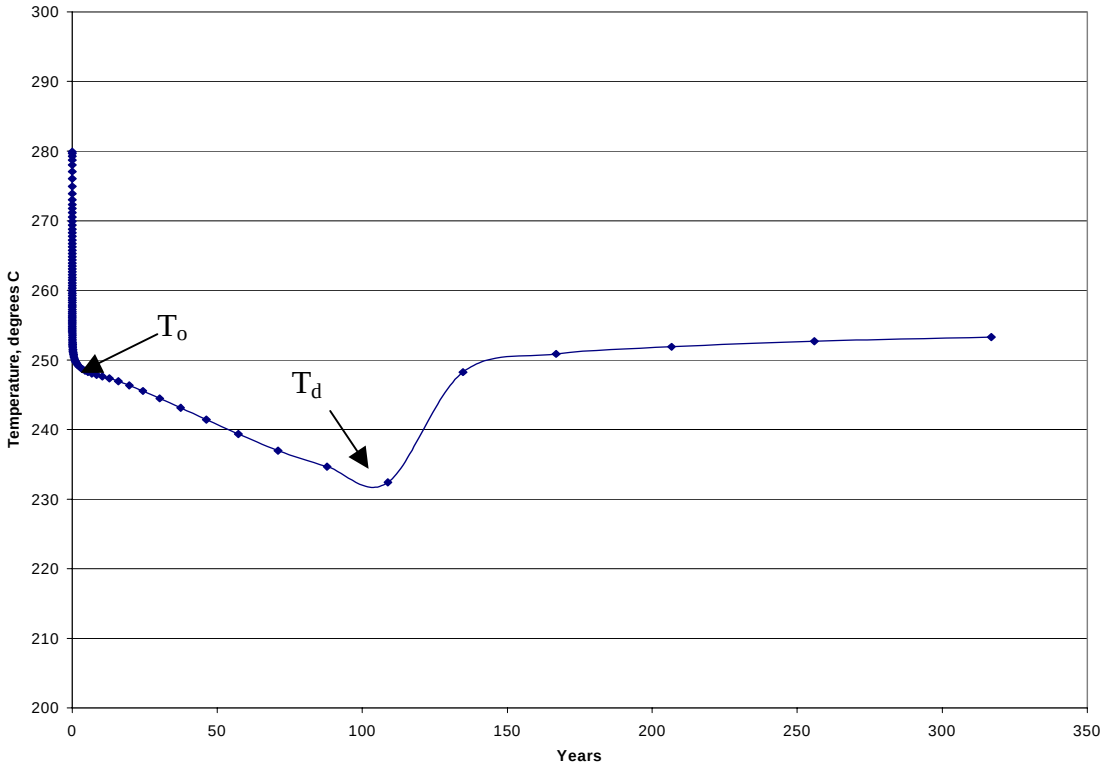

Figure 2-11: Temperature values over a 315 year exploitation period for the TOUGH2 simulated two-phase radial model, irreducible water saturation = 0.3, with initial temperature, T_o and dry-out temperature, T_d indicated.

The zero-dimensional model, as expressed in Equation 2-5 with reservoir properties used in Table 2-1, gives a close approximation of the in-situ water saturation used in the simulation. This means that the assumptions taken in the zero-dimensional model can closely approximate the conditions in actual geothermal wells, therefore, this method is useful to calculate the in-situ water saturation in the Geyser wells.

Using the T_o and T_d values from Figure 2-9:

$$s_o = \frac{(1-\phi)}{\phi}\frac{\rho_r c_r (T_o - T_d)}{\rho_w (h_s - h_w)|_{T_o}} = \frac{(1-0.05)}{0.05}\frac{\left(2600\,{}^{kg}/_{m^3}\right)\left(0.485\,{}^{kJ}/_{kgC}\right)(250^oC - 232^oC)}{799.1689\,{}^{kg}/_{m^3}\left(2800.4\,{}^{kJ}/_{kg} - 1085.78\,{}^{kJ}/_{kg}\right)} = 0.31$$

Using the T_o and T_d values from Figure 2-10:

$$s_o = \frac{(1-\phi)}{\phi}\frac{\rho_r c_r (T_o - T_d)}{\rho_w (h_s - h_w)|_{T_o}} = \frac{(1-0.05)}{0.05}\frac{\left(2600\,{}^{kg}/_{m^3}\right)\left(0.485\,{}^{kJ}/_{kgC}\right)(246^oC - 233^oC)}{805.1\,{}^{kg}/_{m^3}\left(2801.36\,{}^{kJ}/_{kg} - 1066.42\,{}^{kJ}/_{kg}\right)} = 0.22$$

2.4. Estimation of the Initial Reservoir Temperature

Figure 2-3 and Figure 2-4 show that, with the temperature-pressure profile of The Geysers wells, unlike with the simulated results, the initial reservoir temperature, T_o, cannot be distinguished so easily. Taking into account the initial sudden drop in the downhole wellbore pressure as a response to production, the stable temperature, T_o, after the early transient period can be estimated by taking the median temperatures in the first few years. Figures 2-12 and 2-13 illustrate this estimation.

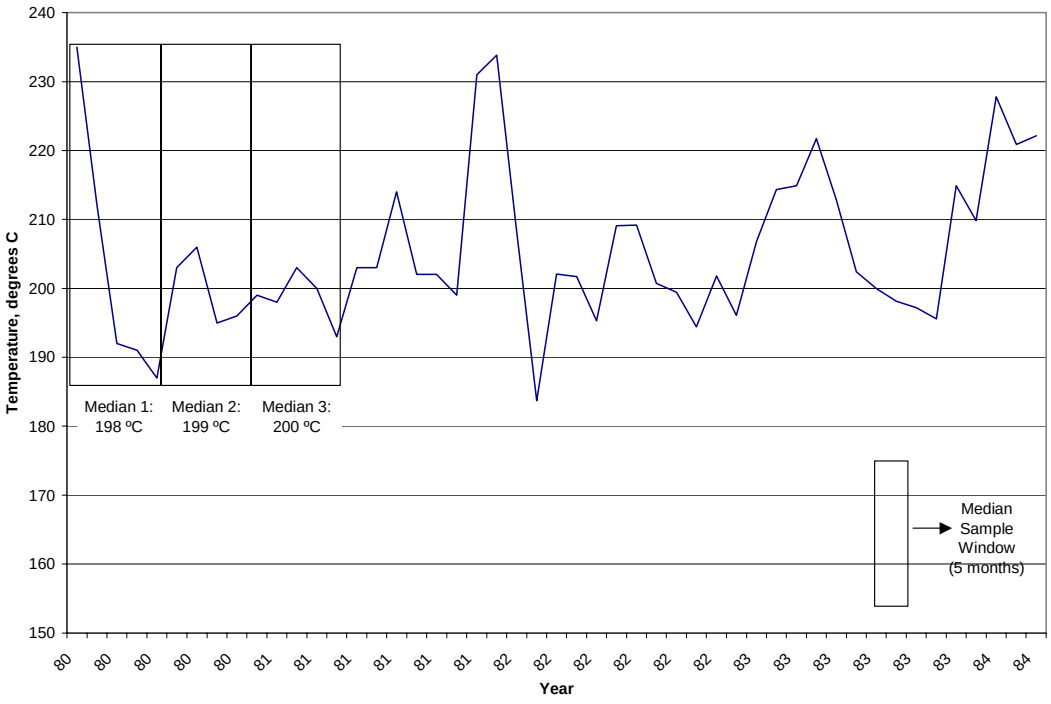

Figure 2-12: Estimation of the initial reservoir temperature T_o, using a median sample window of 5 months for McKinley 1. The estimated T_o is 201.5 ºC.

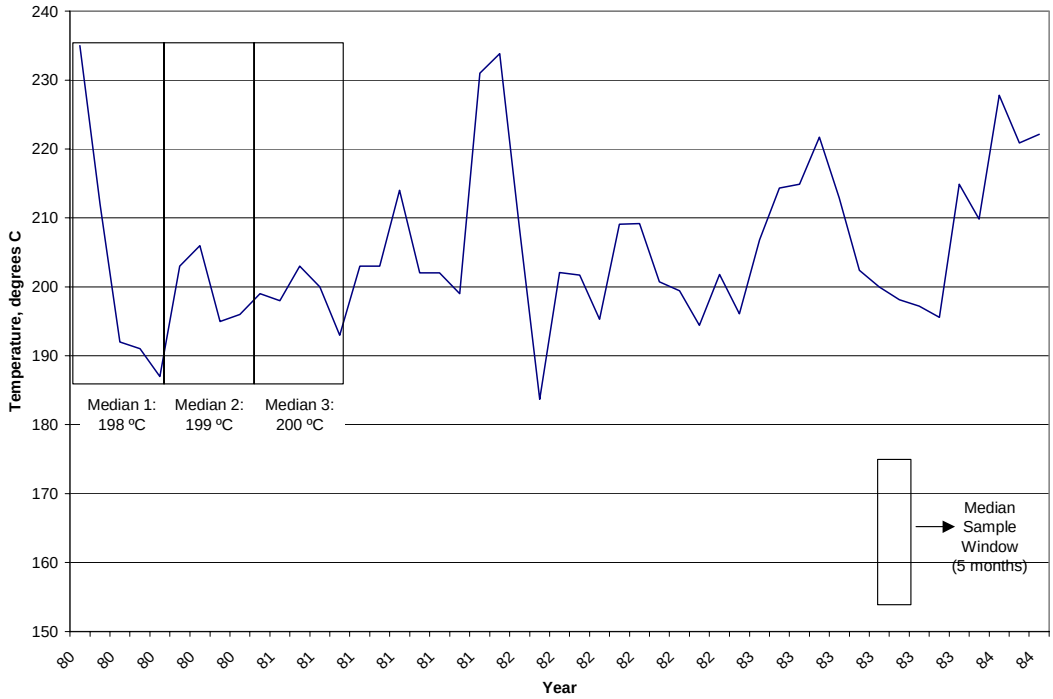

Figure 2-13: Estimation of the initial reservoir temperature T_o, using a median sample window of 5 months for Thorne 1. The estimated T_o is 199 ºC.

2.5. Estimation of Dry-out Temperature

The dry-out temperature can be estimated by acknowledging the fact that this temperature is found where the direct relationship of the temperature and pressure ends, and where the inverse relationship begins, as observed in the determination of the T_d in the simulation case. To see this, consider Figure 2-1 and Figure 2-2. The region of the pressure-temperature profile following the saturation curve corresponds to the period of direct relationship in the pressure and temperature values, and the values below the elbow correspond to the inverse relationship. Figures 2-14 and 2-15 illustrate the relationships that are present with pressure and temperature values, as seen in the computation of the correlation function *R*. using a five-point moving window. A correlation function value *R* of 1 signifies positive correlation, while an *R* of –1 signifies a negative correlation.

It can be seen from these figures that a good part of the left side of either graph has a generally positive correlation. The right side, on the other hand, fluctuates from positive to negative correlation, although the relationship is largely inverse.

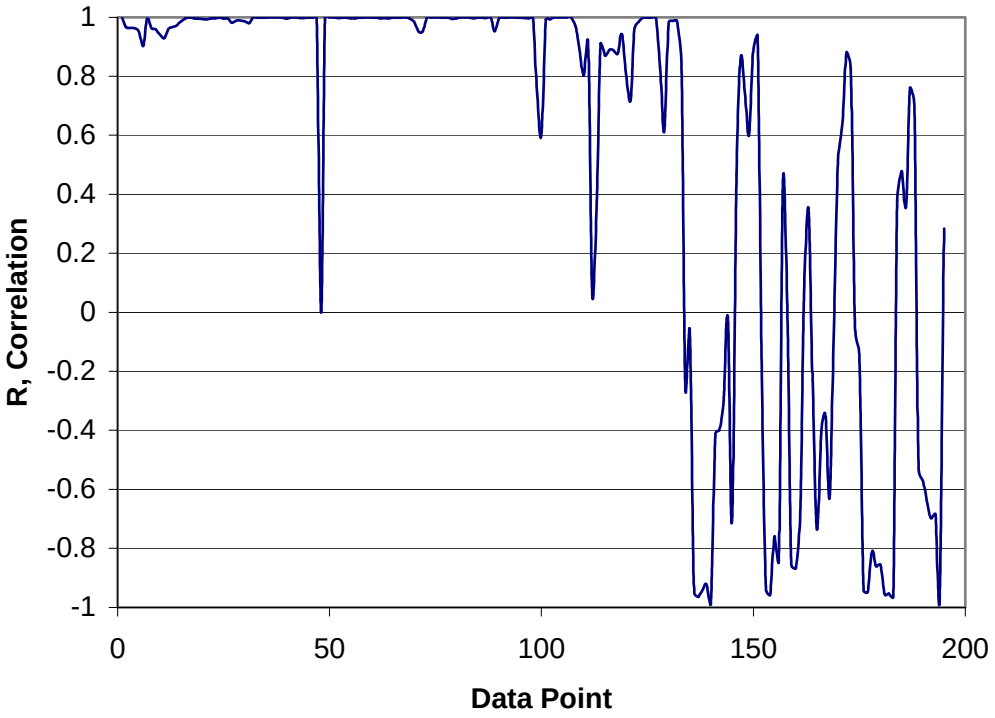

Figure 2-14: Correlation between temperature and pressure data points for McKinley 1.

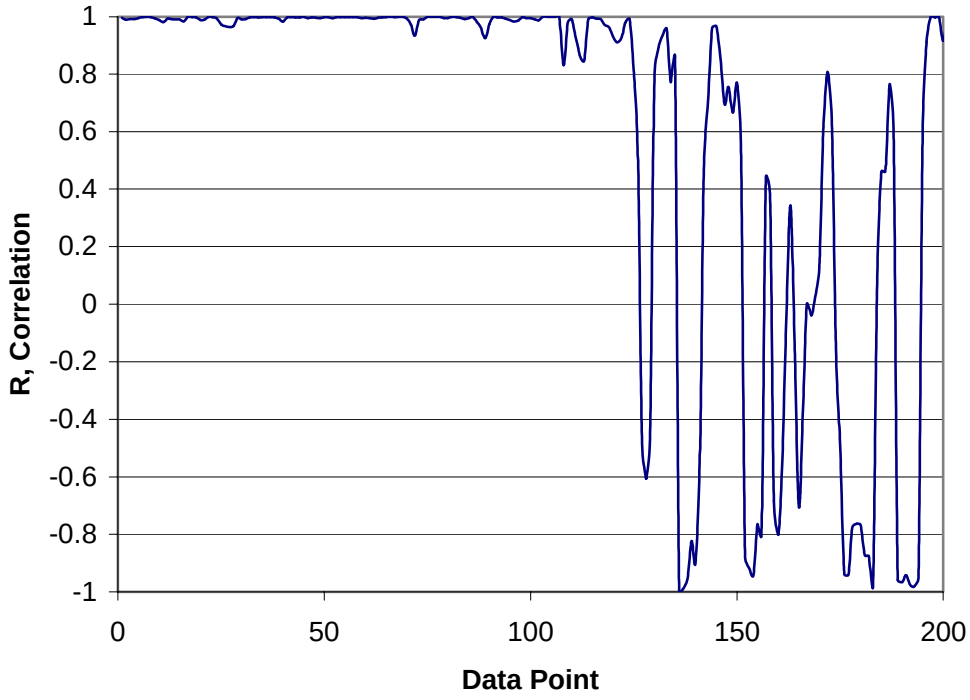

Figure 2-15: Correlation between temperature and pressure data points for Thorne 1.

We can estimate this transition point numerically by recognizing that, at the values of positive correlation, the temperature and pressure values obey the saturation curve. The saturation curve values are generated using the Clausius-Clapeyron equation, given by Equation 2-6.

$$\ln p = -\frac{\Delta h_{vap}}{R_g T} + C \tag{2-6}$$

This equation includes the Δh_{vap}, which is the heat of vaporization of water, and R_g, the universal gas constant. Therefore, we can estimate the time when the positive correlation zone ends, by analyzing the point at which the values of temperature and pressure history stop following the Clausius-Clapeyron equation.

Figures 2-16 and 2-17 show the plot of the saturation pressure values computed from the corresponding historic well temperature values, in comparison to the historic pressure well values. We can see that there are points at which the well pressure values start to deviate from the saturated values, as indicated by the arrows. These points can also be used to estimate the point of dry-out.

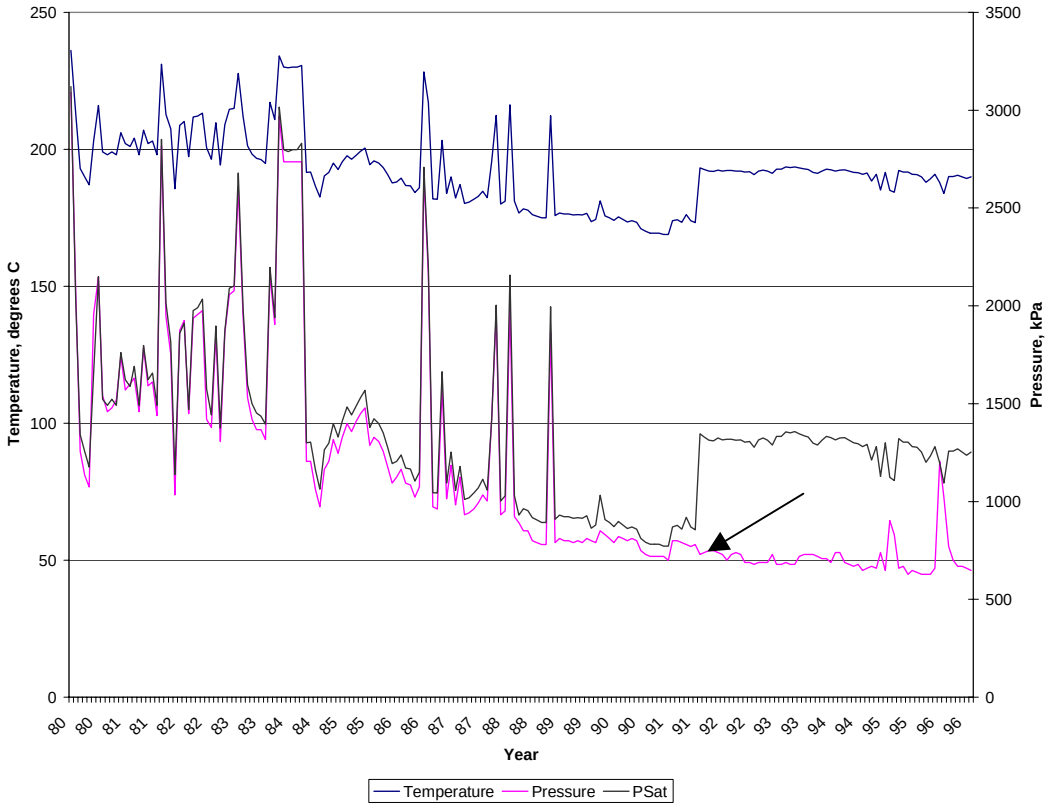

Figure 2-16: Saturated pressure values calculated from well temperature values and pressure values for the McKinley 1 well.

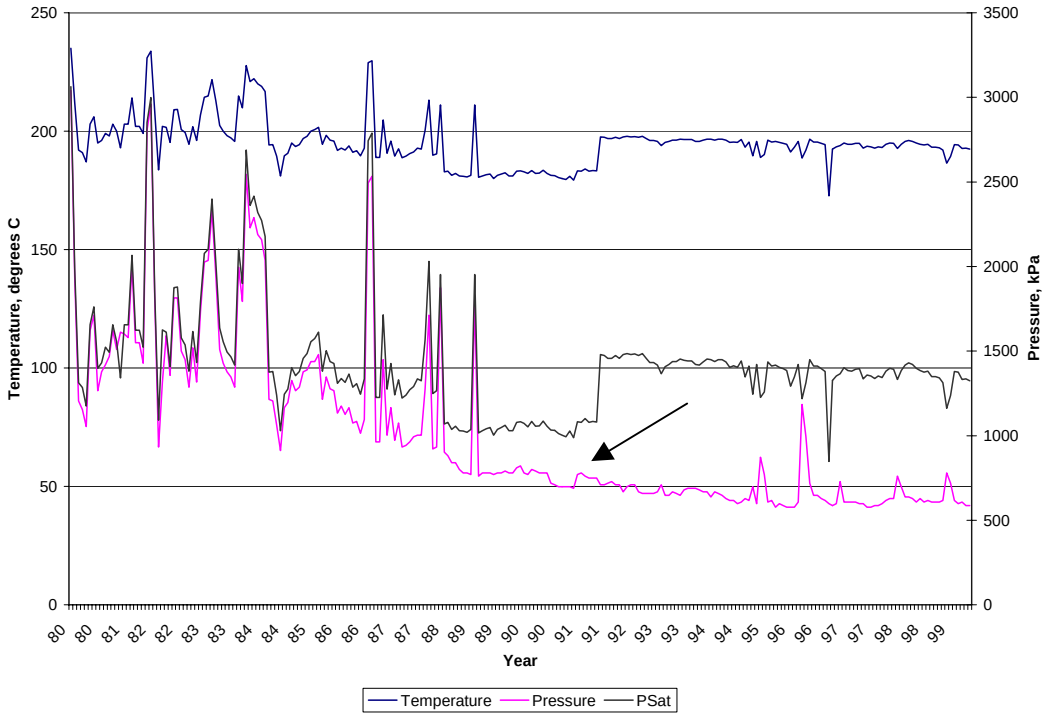

Figure 2-17: Saturated pressure values calculated from well temperature values and pressure values for the Thorne 1 well.

The Clausius-Clapeyron equation can be seen as a straight line by plotting ln(p) vs. 1/T. We can therefore extend this realization to the well data, assuming the elbow will not follow this straight line. Figure 2-18 shows this plot. We can therefore extend this realization to the well data, assuming the elbow will not follow this straight line. Figures 2-19 and 2-20 illustrate this premise, with the first part of the well data generally agreeing with the proposed linear relationship, and second part, the elbow, straying away from the line. The point which separates these two parts will be the dry-out temperature, T_d.

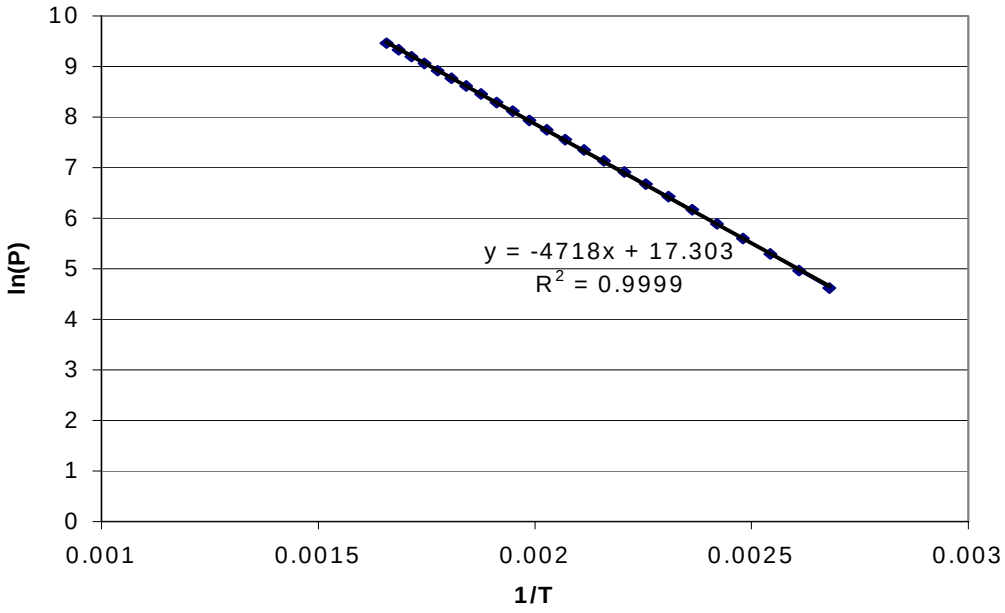

Figure 2-18: Plot of ln(p) vs. 1/T based on the Clausius-Clapeyron Equation.

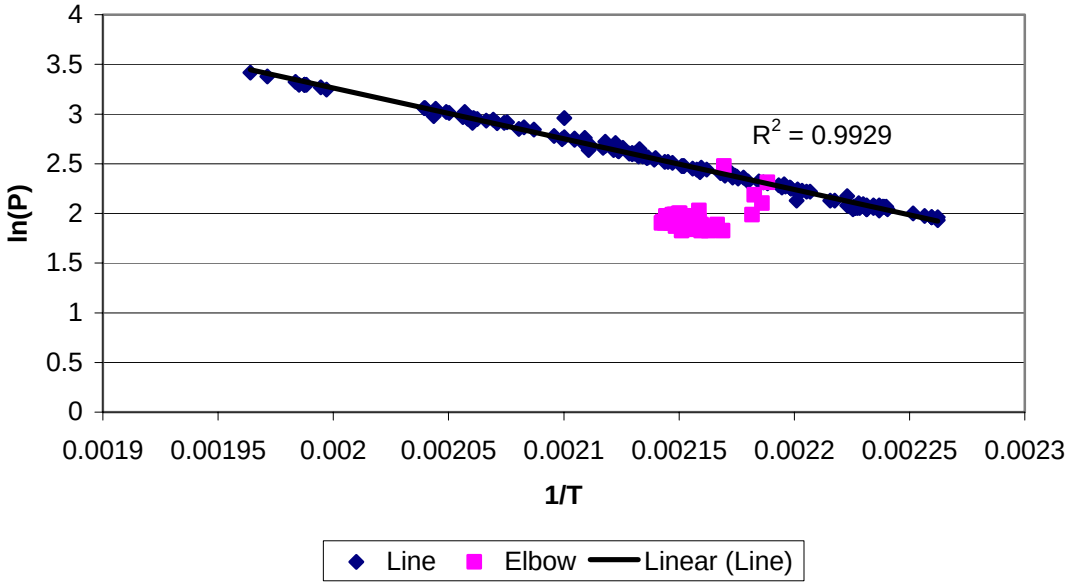

Figure 2-19: Plot of ln(p) vs. 1/T of the McKinley 1 pressure and temperature values to determine the dry-out temperature. The estimated T_d is 193.2 ºC.

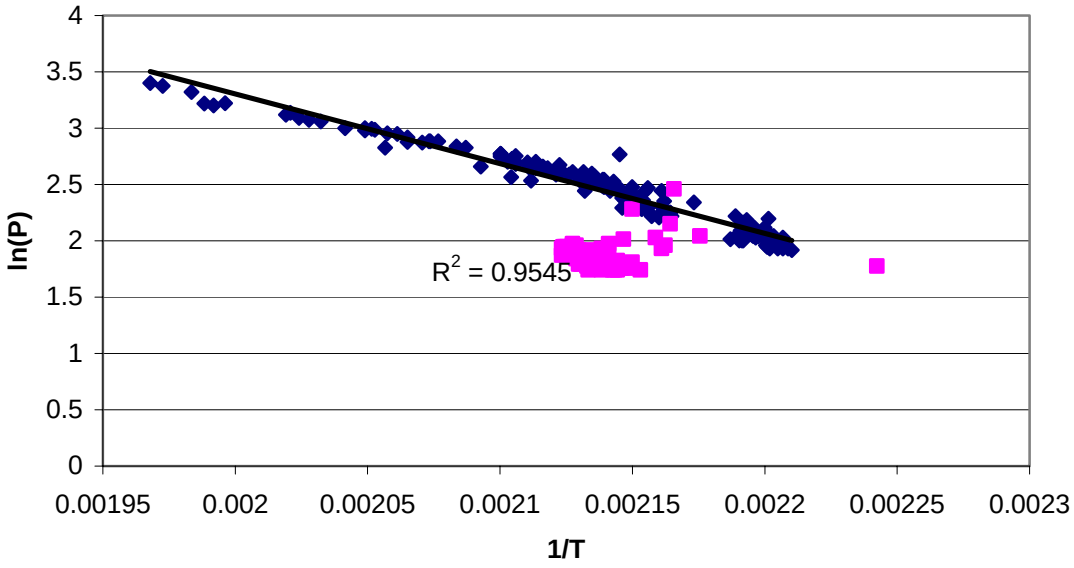

Figure 2-20: Plot of ln(p) vs. 1/T of the Thorne 1 pressure and temperature values to determine the dry-out temperature. The estimated T_d is 197.6 ºC.

Chapter 3

3. Estimated In-Situ Saturation Results

Before we use Equation 2-5 to calculate the in-situ saturation from the well production data for all the well in the database, we must know the various properties of the reservoir rock as well as the downhole initial and dry-out reservoir temperatures.

3.1. Evaluation of Temperature

The temperature data in the production database are derived from wellhead measurements. Since we need to know the downhole temperature rather than the wellhead temperature in order to calculate the saturation, a way to calculate the downhole temperature from the wellhead temperature is needed.

Horne (1988) describes a way to estimate the wellbore temperature and heat losses that facilitate the calculation of temperature profiles along a geothermal well. The equation for the evaluation of the temperature in a producing geothermal well is:

$$T = (T_{BH} - ay) + aA\left(1 - e^{-y/A}\right) + (T_O - T_{BH})e^{-y/A} \tag{3-1}$$

where y is the distance upwards from the bottom of the well, T is the temperature needed at the given depth, T_O is the inflowing fluid temperature, T_{BH} is the downhole reservoir temperature, and a is the geothermal gradient. The parameter A is the diffusion depth which can be estimated by:

$$A(t) = \frac{Wcf(t)}{2\pi k} \tag{3-2}$$

where W is the mass flowrate, c is the thermal heat capacity of the fluid which is assumed to be constant, k is the thermal conductivity of the formation, and $f(t)$ is a dimensionless time function representing the transient heat transfer to the formation. For flowing time greater than 30 days, we can use an estimation of $f(t)$ by the equation:

$$f(t) = -\ln\frac{r}{2\sqrt{\alpha t}} - 0.29 \tag{3-3}$$

where α is the thermal diffusivity of the formation and r is the radius of the casing.

Since we are interested in calculating the bottomhole temperature from the given wellhead temperature, we set T in Equation 3-1 as T_{WH}, which is the wellhead temperature. Assuming the fluid temperature coming from the bottomhole is equal to T_{BH}, we get an equation that will be used for the evaluation of the bottomhole temperature in a producing well under single-phase flow:

$$T_{BH} = (T_{WH} + ay) - aA\left(1 - e^{-y/A}\right) \tag{3-4}$$

Thermal properties assumed for these calculations were derived from Walters and Combs (1989). Data on mass flowrate and flowing times were derived from the database. Depth of the well and the casing size were derived from well completion descriptions furnished by the companies that drilled the wells.

Figure 3-1 and Figure 3-2 plot the downhole temperatures and the wellhead temperatures, as well as the difference between these two temperatures, for McKinley 1 and Thorne 1, respectively.

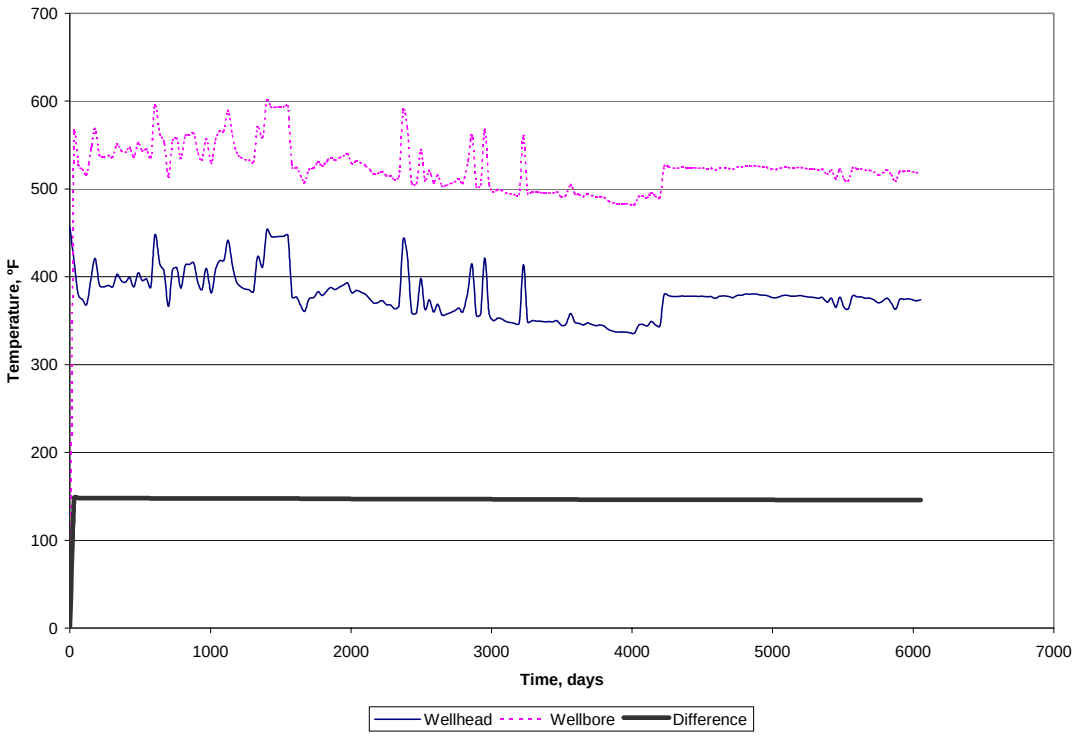

Figure 3-1: Wellhead and wellbore temperatures for McKinley 1 well.

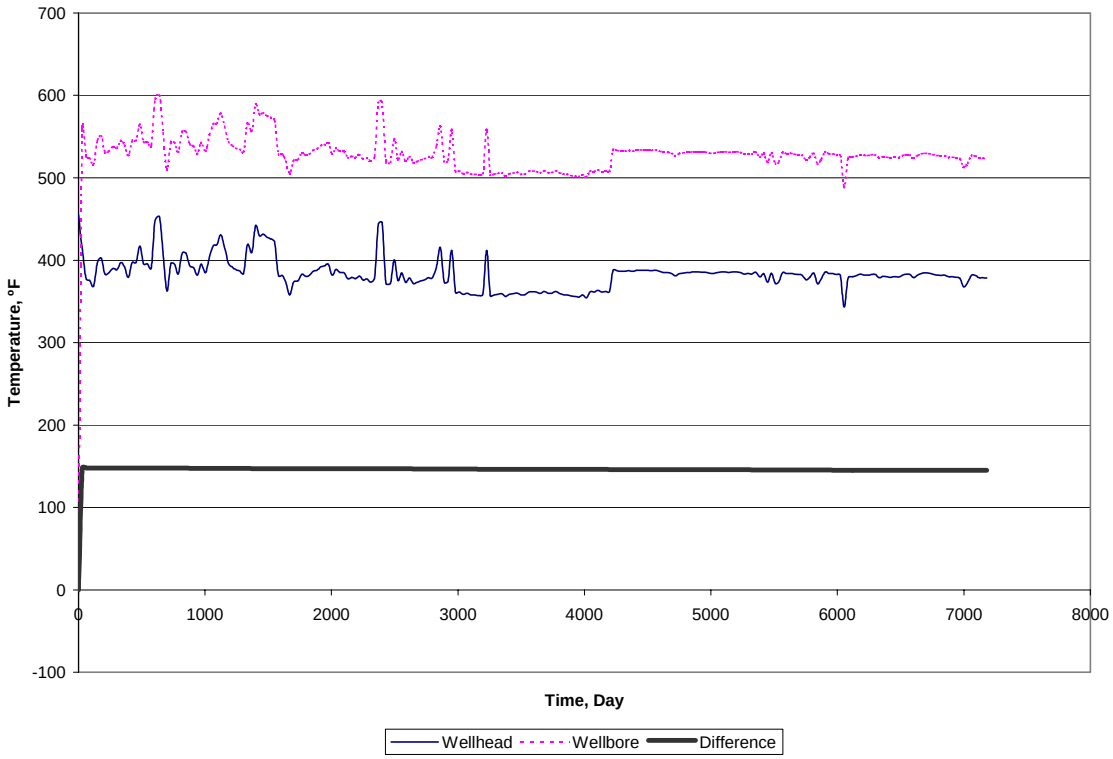

Figure 3-2: Wellhead and wellbore temperatures for Thorne 1 well.

The calculated difference between the wellbore and the wellhead temperature was between 146.2ºF and 147.99ºF for McKinley 1 and 146.1ºF and 147.99ºF for Thorne 1. This meant a 1.79 and 1.93 degree relative difference between the initial and dry-out temperatures for McKinley 1 and Thorne 1, respectively. The average difference in the initial and dry-out temperatures calculated for all the wells was 2.24 ºF, with a range of 0.267 to 7.11 ºF. This produced average percent increase in the estimated saturation values of about 12%, with a range of 0.11.

From the downhole temperature calculations for both wells, a range of values from 480 ºF to about 600 ºF were computed. This is consistent with the findings from Pham and Menzies (1993) that suggests a temperature of 470 ºF at saturation conditions, and temperatures greater than 500 ºF for depths greater than 1800 meters.

3.2. Evaluation of Other Properties

For the other reservoir rock properties, we searched existing literature to find values. The predominant reservoir rock is metagraywacke. Quoted values for the specific heat of this rock have ranged from 917 J/kg ºC (Barker et al. 1991), to values of 1000 J/kg ºC (Taylor, 1992 and Mossop et al. 1997). We assumed a specific heat of 960 J/kg ºC.

For rock density, Mossop et al. gave a Geysers rock density of 2700 kg/m^3. Estimates of Brown (1989) for graywacke densities range from 2660 kg/m^3 to 2770 kg/m^3. A rock density of 2700 kg/m^3 was be used for this study.

The rock porosity at the Geysers is fracture-related. Porosities of reservoir graywacke cores sampled by Gunderson (1992) ranged from a low of 0.6 percent to a high of 5.8 percent. Duba et al. (1992), used electrical properties of The Geysers as an indicator of porosity distribution, and the study derived a range of 0.973% to 6.54 %. Due to the presence of fractures, however, the actual bulk porosities are likely to be higher than the core samples used to estimate porosity of the rock matrix.

We investigated the effect of varying porosities on the calculation of in-situ saturation. Table 3-1 gives values of saturation ranges and average saturation values for various values of porosity and the other assumed reservoir rock properties.

Table 3-1: In-situ saturation values calculated from various porosity values.

	Porosity					
Saturation	**5.7 %**	**6 %**	**7 %**	**8 %**	**9 %**	**10 %**
Average	0.526	0.499	0.423	0.366	0.322	0.286
Low Value	0.207	0.196	0.167	0.144	0.127	0.113
High Value	0.999	0.946	0.803	0.695	0.598	0.544

The lowest assumed porosity of 5.7 % gives us saturation values ranging between 0.2 and close to 1. The highest assumed porosity, 10%, yielded a saturation value range of 0.11 to 0.54. Results from Willamson (1990) used history matching to infer an in-situ saturation of 82% for The Geysers. Pham et al. (1993) found that values of in-situ saturation ranging between 55% to 90% were necessary to obtain matches between simulated pressure values and field pressure values in their numerical model of the Geysers. In view of these findings, we used a porosity of 5.7% in our analysis.

3.3. Calculation of Saturation Values

Table 3-2 shows the calculated values of the saturations, as well as the values for T_o and T_d used to arrive at this result. We identified 177 wells in the database that show the presence of the dry-out point, therefore allowing the computation of the saturation values. The remaining 179 wells have data that are too sparse to observe any relationships.

Table 3-2: Calculated in-situ saturation values for 177 wells in The Geysers database.

Well Name	So	To	Td
Abel 1	0.505	196	178.3
Angeli 2	0.417	186.1	171.1
Angeli 3	0.407	186.1	170.6
Beigel 1	0.399	188.9	176.7
Beigel 2	0.535	195.6	175.6
Beigel 3	0.504	186.7	167.8
CA-1862 15A-21	0.999	208.3	172.8
CA-1862 15B-21	0.471	192.2	173.3
CA-1862 62D-29	0.370	193.7	178.9
CA-5636 23B-22	0.440	182.6	164.4
CA-5636 23G-22	0.483	187.6	167.9
CA-5636 23H-22	0.333	184.4	170.7
CA-5636 36C-22	0.386	181.9	165.9
CA-5636 68B-21	0.861	196.6	162.5
CA-5636 68D-21	0.931	197.9	161.2
CA-5636 74G-21	0.345	177.8	163.3
CA-5636 74H-21	0.331	177.4	163.5
CA-5636 87A-21	0.391	180.5	164.2
CA-5636 87B-21	0.553	182.3	159.4
CA-5636 87C-21	0.544	182.9	160.4
CA-5636 87D-21	0.874	197.4	162.9
CA-5636 87G-21	0.552	186.3	163.7
CA-5637 68-21	0.728	193.8	164.7
CA-5639 14A-27	0.401	201.12	186.7
CA-5639 15-28	0.580	191.1	169.4
CA-5639 15A-28	0.479	187.2	168.9
CA-5639 15C-28	0.311	181.7	170
CA-5639 15D-28	0.315	181.7	169.4
CA-5639 36-28	0.349	181.7	167.2
CA-5639 42-33	0.504	186.7	167.2
CA-5639 44-28	0.488	190	171.7
CA-5639 44A-28	0.505	187.2	168.3
CA-5639 44B-28	0.600	193.9	171.1
CA-5639 53-33	0.600	192.8	169.4
CA-5639 63-29	0.483	192.8	174.4
CA-5639 63A-29	0.766	197.8	168.9
CA-5639 63B-29	0.429	190.6	173.3
CA-5639 85-28	0.431	188.9	173.3
CA-5639 85A-28	0.398	187.8	172.8
CA-956A 56-34	0.626	194	172.7
CA-956A 56C-34	0.559	198.3	176.3
CA-956A 86-34	0.386	200.4	188.4
CA-958 37-34	0.644	197	175.2
CA-958 37A-34	0.553	196.5	181.7

Well Name	So	To	Td
CA-5634 21B-12	0.439	190.6	173.9
CA-5634 21D-12	0.443	190	173.3
CA-5634 32-12	0.379	186.1	171.7
CA-5634 32A-12	0.518	191.1	171.7
CA-5634 32B-12	0.424	187.8	172.2
CA-5634 32C-12	0.389	187.2	172.8
CA-5634 45B-12	0.425	187.8	171.1
CA-5634 52-11	0.672	200.6	176.1
CA-5635 117-19	0.570	192.2	170.6
CA-5635 123-19	0.381	183.3	169.4
CA-5635 94A-19	0.493	190.6	172.2
CA-5635 94B-19	0.702	197.2	171.1
CMHC 5	0.347	187.8	175.6
Coleman 1A-5	0.447	204.2	187.2
DX State 4596 22A	0.979	208.9	173.9
DX State 4596 23	0.570	193.3	172.8
DX State 4596 25	0.490	190.6	172.8
DX State 4596 27	0.475	187.8	172.8
DX State 4596 4	0.515	188.3	169.4
DX State 4596 40	0.455	191.1	174.4
DX State 4596 41	0.399	191.1	175
DX State 4596 42	0.654	197.8	174.4
DX State 4596 50	0.457	200.6	185
DX State 4596 56	0.432	186.4	171.1
DX State 4596 58	0.580	194.4	173.9
DX State 4596 59	0.586	195	173.3
DX State 4596 60	0.659	197.2	173.9
DX State 4596 62	0.299	183.3	171.7
DX State 4596 68	0.493	192.2	173.9
DX State 4596 69	0.642	197.2	174.4
DX State 4596 73	0.367	188.3	174.4
DX State 4596 74	0.351	185	172.2
DX State 4596 75	0.441	188.3	172.2
DX State 4596 76	0.666	198.9	173.3
DX State 4596 82	0.300	185.6	173.3
DX State 4596 85	0.525	193.3	172.8
Francisco 2-5	0.528	190.6	170
GDC 1	0.458	190	172.2
GDC 10	0.618	193.9	173.9
GDC 11	0.622	195.6	174.4
GDC 19	0.449	190	172.8
GDC 2	0.424	186.1	172.2
GDC 20-29	0.592	194.4	174.4
GDC 24	0.531	192.8	172.8

Well Name	So	To	Td
CA-958 37B-34	0.404	198.2	182.3
CA-958 37C-34	0.478	200.4	181.7
CA-958 56A-34	0.485	193	177.1
CA-958 56B-34	0.619	194.8	172.2
CA-958 86A-34	0.718	198.7	173.4
D & V 1	0.643	194.4	171.1
D & V 11	0.498	190	171.1
D & V 12	0.789	198.9	171.7
D & V 13	0.675	195.6	170.6
D & V 15	0.582	192.8	172.2
D & V 16	0.583	192.8	171.7
D & V 2	0.612	206.7	187.2
D & V 6	0.407	186.1	170
D & V A-2	0.994	202	168.8
D & V A-3	0.899	202	171.6
D & V A-4	0.840	199.9	169.1
GDC 23	0.439	185.6	169.4
GDC 29	0.462	190	173.9
LF State 4597 1	0.582	192.2	171.7
LF State 4597 10	0.749	195.6	168.3
LF State 4597 13	0.454	185	168.3
LF State 4597 37	0.641	193.3	168.9
LF State 4597 38	0.368	182.2	168.3
LF State 4597 42	0.406	187.8	172.2
LF State 4597 48	0.330	185	172.2
LF State 4597 49	0.328	185	172.2
McKinley 1	0.508	193	173.9
McKinley 10	0.612	203.7	182.5
McKinley 11	0.461	197.7	181
McKinley 12	0.493	192.4	175.2
McKinley 13	0.545	195.6	175.2
McKinley 15	0.750	206.6	177.9
McKinley 3	0.636	201	180.2
McKinley 4	0.623	204	183.6
McKinley 9	0.594	201.9	180.7
MLM 1	0.619	205	186
MLM 2	0.565	205	184.9
Modini 1	0.534	206.1	187.8
Modini 3	0.477	206.1	187.8
Modini 4	0.745	198.9	173.3
Thorne 1	0.446	199	183.4
Thorne 6	0.545	197	177.9
Tocher 3	0.573	197	175.6
CA-5634 21-12	0.468	191.7	174.4
CA-5634 21A-12	0.516	192.2	172.8

Well Name	So	To	Td
GDC 25	0.478	190	172.8
GDC 30	0.255	181.7	171.1
GDC 32A-13	0.668	192.8	168.3
GDC 66-12	0.706	194.4	170
GDC 7	0.529	189.4	171.7
GDC 8	0.207	193.3	185
GDC 85-12	0.583	185	166.1
GDC 86-12	0.762	195.6	169.4
GDC 9	0.489	190	173.9
Geyser Gun Club 6	0.492	193.3	175.6
Geyser Gun Club 8	0.396	190.6	176.1
Happy Jack 11	0.437	185.6	170
LF State 4597 12	0.442	185	169.4
LF State 4597 14	0.464	185	168.9
LF State 4597 18	0.543	192.8	172.8
LF State 4597 27	0.413	187.2	172.2
LF State 4597 28	0.496	190.6	172.2
LF State 4597 29	0.433	188.3	172.2
LF State 4597 31	0.425	185	169.4
LF State 4597 34	0.534	192.2	172.8
LF State 4597 36	0.466	189.4	172.2
LF State 4597 4	0.644	190.6	168.3
LF State 4597 5	0.735	196.7	172.8
Ottoboni St 4596 13	0.454	190.6	173.9
Ottoboni St 4596 14	0.328	185.6	174.4
Ottoboni St 4596 16	0.366	185	172.2
Ottoboni St 4596 18	0.445	187.2	171.2
Ottoboni St 4596 23	0.614	190.6	171.1
Ottoboni St 4596 24	0.568	186.7	170
Ottoboni St 4596 29	0.346	187.2	173.9
Sulphur Bank 10	0.487	177.8	159.4
Sulphur Bank 11	0.756	186.1	162.2
Sulphur Bank 14	0.539	177.2	160.6
Sulphur Bank 17	0.781	188.9	158.4
Sulphur Bank 20	0.517	187.2	166.1
Sulphur Bank 21	0.423	182.2	167.2
Sulphur Bank 22	0.504	185	166.7
Sulphur Bank 23	0.635	192.2	166.7
Sulphur Bank 24	0.727	197.8	171.1
Sulphur Bank 26	0.426	187.2	171.7
Sulphur Bank 27	0.534	190.6	171.7
Sulphur Bank 28	0.436	190.6	174.4
Sulphur Bank 30	0.522	187.2	167.8
Sulphur Bank 31	0.406	190	174.4
Sulphur Bank 8	0.639	185.6	159.4

To understand the spatial trends of saturation values in the Cartesian plane, we mapped out different types of wells we classified. Figure 3-3 shows an aerial view of a contour plot made by the saturation values. The two boxes located in the upper-left region of the plot, and the lower-left region of the plot correspond to the Northwest (NW) and Southeast (SE) zones, respectively. We can see that in the SE location, we have mostly blue colors, signifying a higher average saturation values (0.55). In the NW location, we see orange and yellow values, indicating that there is a concentration of lower average saturation value in this zone (0.5).

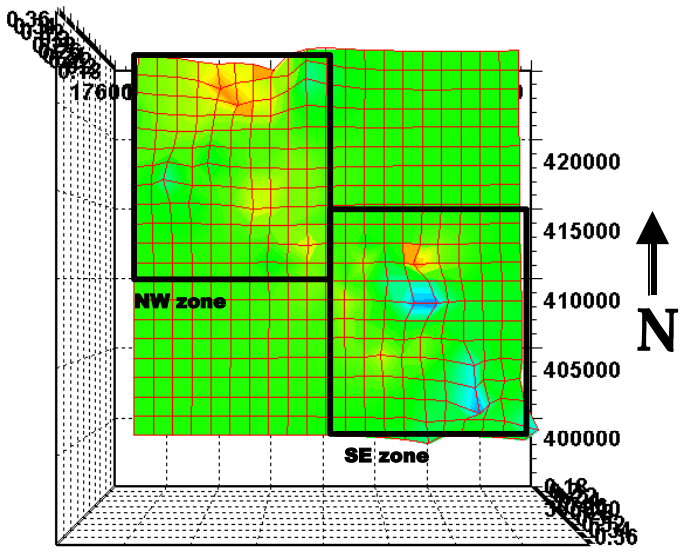

Figure 3-3: Aerial view contour plot of the saturation values on the Cartesian plane of the 177 superheated Geyser wells.

3.4. Other Wells

We identified wells that do not have a discernable change in trend, and therefore infer that these wells have not reached superheat. Figure 3-4 shows an example of such a well, and as we can see the relationship between the pressure and temperature is direct all throughout the history. We identified 147 wells that exhibit this trend.

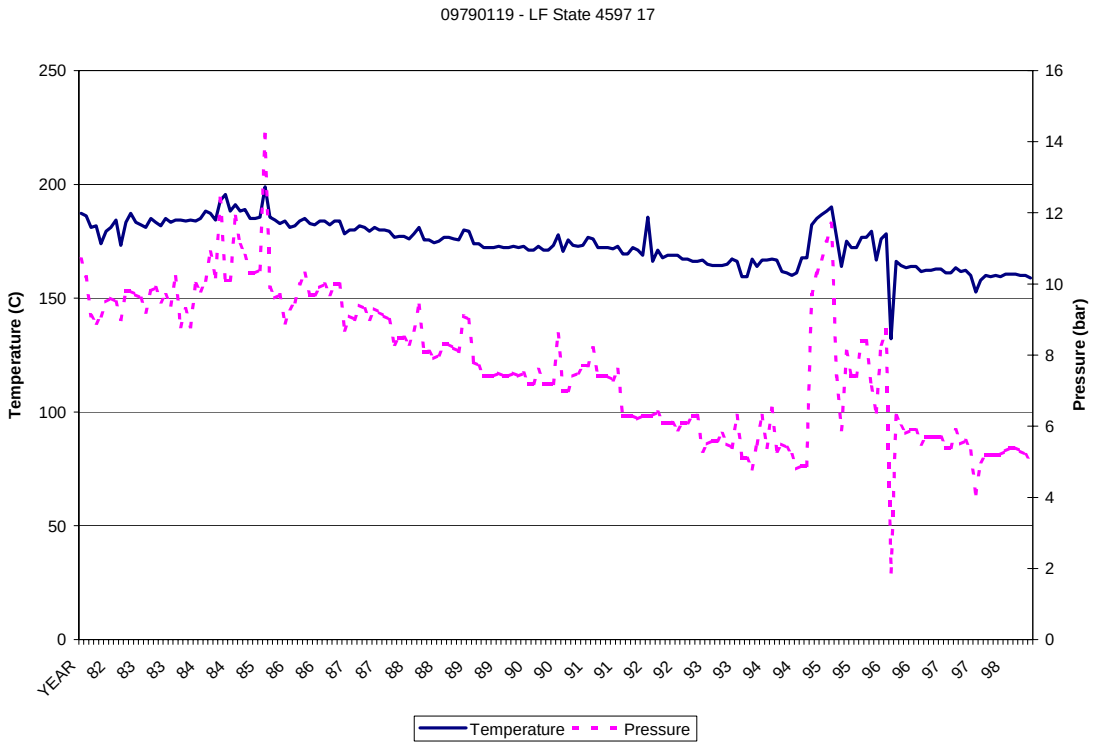

Figure 3-4: Temperature and pressure values history for a well with no dry-out point.

The remaining 179 wells have data that are too sparse to observe any relationships. An example of such a well is shown in Figure 3-5. We also identified 25 injection wells from the database.

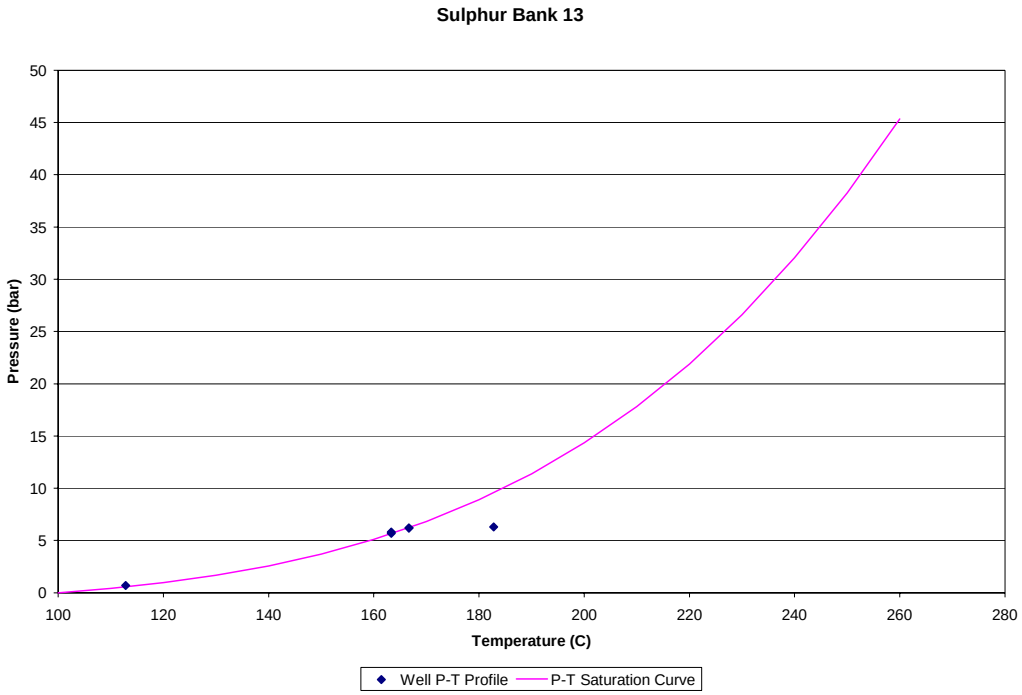

Figure 3-5: Pressure-temperature profile of a well with sparse data.

Figure 3-6 shows the plot of wells that have not yet reached superheat, which we call "saturated" wells, on the Cartesian plane. The NW zone has 64% of all the saturated wells, indicating that there is a higher number of saturated wells in the NW zone than in the SE zone.

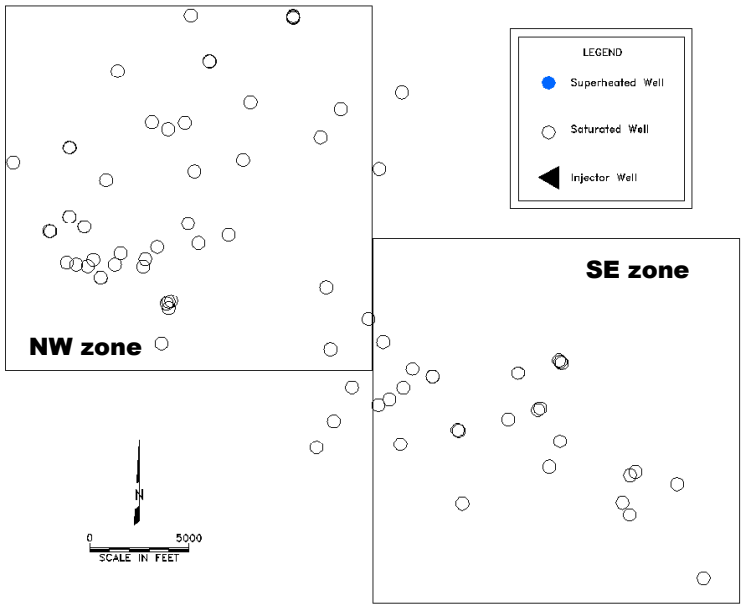

Figure 3-6: : Locations of the saturated wells.

Chapter 4

4. Effect of Reinjection

To investigate the possible effect of an increase of the calculated saturation values due to reinjection, we plotted the locations of the injection wells in the Cartesian plane. Figure 16 shows the plot, and we can say that these wells are evenly distributed throughout the field.

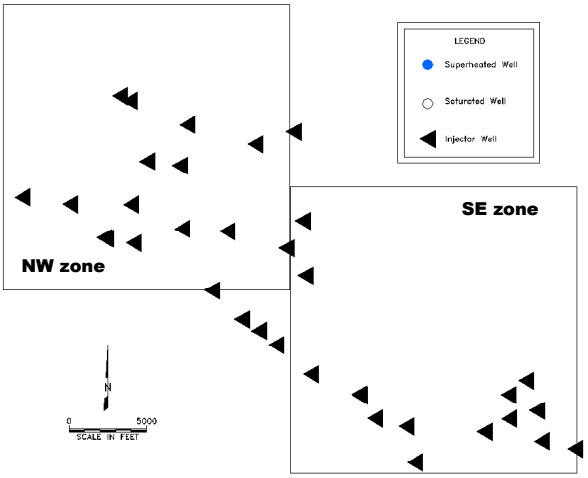

Figure 4-1: Locations of the injection wells.

4.1. Simulation of Reinjection

We analyzed the trends presented so far further by simulating the influence of reinjection in the vicinity of a producing well using TOUGH2. In the simulation, we injected water at constant flowrate and 20ºC temperature to the grid cell farthest from the center of the radial model used in previous simulations. We used a value of 0.3 for the in-situ water saturation and we investigated whether reinjection affects the estimates of this value from the zero-dimensional model. The temperature and pressure profiles for this simulation are plotted in Figure 4-2.

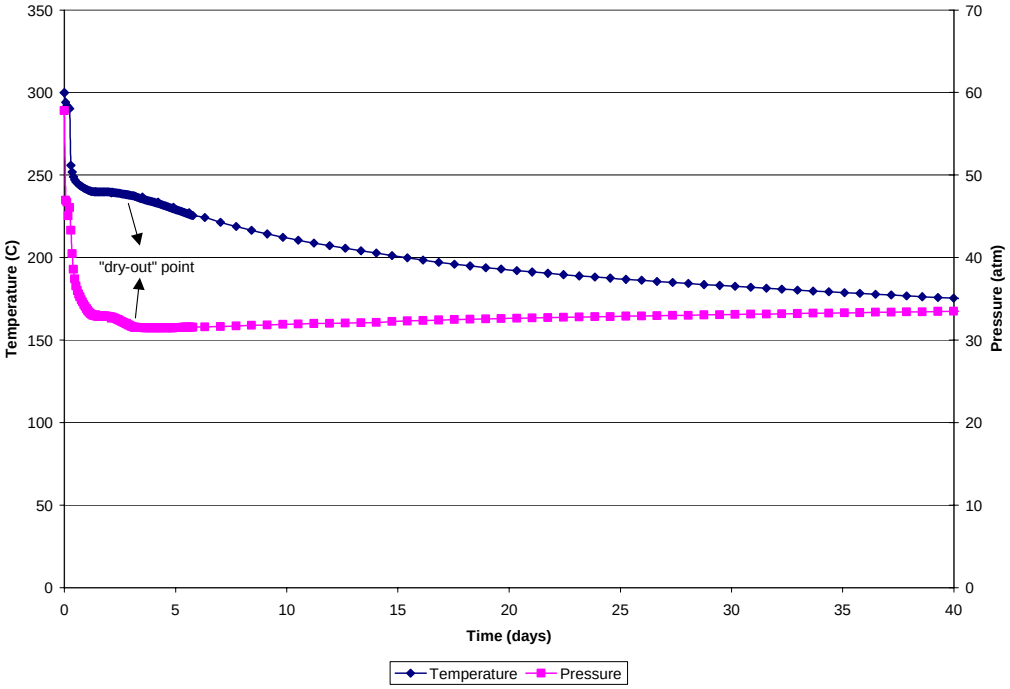

Figure 4-2: Pressure-temperature history showing the dry-out point for a simulation run showing reinjection.

In Figure 4-2 we have identified the zones of direct and inverse relationships, therefore we can use this to identify the T_o and T_d values to calculate the in-situ water saturation from the zero-dimensional model. If we calculate the in-situ saturation, the original saturation of 0.3 appears to increase to 0.36, indicating that indeed reinjection increases estimated value of the in-situ water saturation in the well.

We might therefore attribute the high saturation values found in the SE zone of the Geysers to be a result of reinjection. It is known that in this zone, we have the presence of an enhanced water supply (from the Lake County waste water project), therefore this, coupled with a lowering of pressure in the zone, contributes to the high apparent saturation values.

4.2. Effect of Reinjection Location

We further investigated the effect of reinjection by varying the flowrate of reinjection and the location of reinjection. We fixed an in-situ saturation as 0.3 in the simulator, with reservoir properties shown in Table 2-1. At the center we put a production well with a production index of 1×10^{-13} operating against a downhole pressure of 1378.6 kPa.

We varied the location of the reinjection by placing reinjection wells in the locations shown in Figure 4-3. The names A31, A51 and A81 correspond to the gridblock number where reinjection occurs The reinjection flowrate was fixed to be 20% of the average

production flowrate from the previous simulation. Table 4-1 summarizes the effect of location on the saturation value of the reservoir.

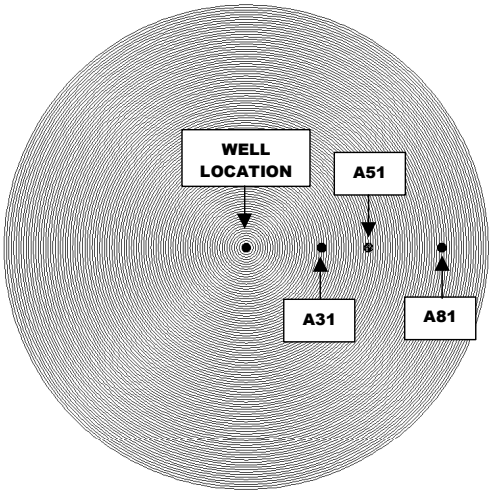

Figure 4-3: Production well and reinjection well locations in the simulation model.

Table 4-1: Effect of location of reinjection well to the in-situ water saturation value.

Gridblock	**S_o**	**T_o**	**T_d**
A31	0.479	300	280
A51	0.455	300	281
A81	0.335	300	286

We can see from the Table 4-1 that A31, the reinjection well nearest to the production well, has the highest apparent saturation value (0.48). The saturation value from the farthest reinjection well (A81), provided us a value of 0.33. We can see from this that the well location affects the calculated saturation value of the well.

4.3. Effect of Reinjection Flowrate

We investigated the effect of flowrate by assuming higher and lower flowrates from the original flowrate of 16% of the original production well case. We placed the wells in block A51. The results are summarized in Table 4-2.

Table 4-2: Effect of flowrate of the reinjection well to the in-situ water saturation value.

Flowrate	S_o	T_o	T_d
0.3 kg/s (4 %)	0.431	300	282
0.8 kg/s (16 %)	0.455	300	281
2 kg/s (40 %)	0.479	300	280

We can see from the Table 4-2 that a higher flowrate means a higher inferred saturation value, and reinjection at 4 % of the production flowrate yields the lowest inferred saturation value.

5. Conclusions

1. Vapor-dominated geothermal reservoirs under exploitation can be depleted locally of water to form a dry or superheated zone.

2. Well performance data history can be used to infer in-situ water saturation.

3. A geothermal reservoir can be said to have dried-out when its pressure-temperature profile deviates from the steam saturation curve.

4. Zero-dimensional models can be used to calculate the in-situ water saturation after identifying the initial reservoir temperature and the dry-out temperature.

5. Based on our estimates, prior to exploitation The Geysers wells had an average in-situ water saturation of 0.55 in the Southwest zone. The wells in the Northwest zone had an average value of 0.5. These values are consistent with inferences made by earlier authors using numerical models of the field.

6. An increase in apparent in-situ saturation is attributable to reinjection of water, and may also be affected by the location and rate of reinjection. This influence may explain the apparently higher in-situ water saturation in the Southwest zone.

Nomenclature

a = geothermal gradient
C = specific heat capacity
c = compressibility
h = enthalpy
k = permeability
k = thermal conductivity
p = pressure
r = radius
R = ideal gas constant
R = correlation value
s = saturation
T = temperature
t = time
y = depth
u = velocity
V = volume
α = thermal diffusivity
ϕ = porosity
μ = dynamic viscosity
ρ = density
ν = kinematic viscosity

BH = bottomhole
d = dry-out conditions
g = gas
o = initial conditions
r = rock
s = steam

vap = vapor

w = water

WH = wellhead

References

Barker, B., Gulati, M., and Riedel, K.L.: "Geysers Reservoir Performance," *Geothermal Resources Council*, Monograph on the Geysers Geothermal Field, Special Report No. 17, pp 167 – 177. 1991.

Barker, B., and Pingol, A.: "Geyser Reservoir Performance – An Update," *Proceedings*, Twenty Second Workshop on Geothermal Reservoir Engineering, Stanford University, California, Stanford, January 27-29, 1997; SGP-TR-155.

Belen, R.P., Jr.. and Horne, R.N.: "Inferring In-Situ and Immobile Water Saturations from Field Measurements", *Geothermal Resources Council*, Trans. **24** (2000).

Bowen, R.: "*Geothermal Resources*," 2nd Edition, Elsevier Science Publishing Co., Inc, New York, 1989.

Brown, J.M.: "Bedrock Geotechnical Properties Affecting groundwater Movement in the U.S. Coast Guard Reservation, Kodiak, Alaska." *Alaska Division of Geological and Geophysical Surveys*, Alaska Pacific University. 1989.

Grant, M., Donaldson, I., and Bixley, P.: "*Geothermal Reservoir Engineering*," Academic Press, Inc., New York, 1982.

Gunderson, R.P.: "Porosity of Reservoir Graywacke at the Geysers," *Geothermal Resources Council*, Monograph on The Geysers Geothermal Field, Special Report No. 17, pp. 89 – 96. 1992.

Horne, R.N.: "Geothermal Energy Assessment", in *Geothermal Reservoir Engineering*, editor E. Okandan, Reidel. 1988.

Mossop, A. and Segall, P.: "Subsidence at the Geysers Geothermal Field, N. California from a Comparison of GPS and Leveling Surveys," *Geophysical Research Letters*, Vol. 24, No. 14, pp. 1839 – 1842. 1997.

Pruess, K.: "TOUGH2 - A General-Purpose Numerical Simulator for Multiphase Fluid and Heat Flow", Report LBL-29400, *Lawrence Berkeley National Laboratory*, Berkeley Calif. (1991).

Taylor, R.E., Shoemaker, R. L., and Groot, H.: "Thermophysical Properties of Selected Rocks: A Report to U.S.G.S.," *TPRL* 271 32 pp., Thermophysical Prop. Res. Lab., Purdue Univ., Indiana, 1982.

Walters, M., and Combs, J.: “Heat Flow Regime in the Geysers-Clear Lake Area of Northern California,” *Geothermal Resources Council,* Trans. **14** (1989)

Williamson, K.H.: “Reservoir Simulation of the Geysers Geothermal Field,: *Proceedings*, Fifteenth workshop on Geothermal Reservoir Engineering, Stanford University, California, January 23 – 25, 1990: SGP-TR-130.

Appendix A

A. TOUGH2 and iTOUGH2 input files for dry-out point simulation

```
*Forward Calculations*
ROCKS----1----*----2----*----3----*----4----*----5----*----6----*----7--
--*----8
GEYSR    2    2600.0       0.05   1.0E-14        0.0        0.0       2.43
485.0
       0.0        0.0       2.43        0.0
    1           0.300     0.000     1.000     0.700
    6           0.000     0.300

START----1----*----2----*----3----*----4----*----5----*----6----*----7--
--*----8
PARAM           12345678901234567890123 4
   29999    99991000301001010004000010000 2.130E-05                  1.0
              1.0E12  1.00E-01                            9.81
     1.E-5
             6420.2E3               280.0                 0.3

MESHMAKER1----*----2----*----3----*----4----*----5----*----6----*----7--
--*----8
RZ2D
RADII
  101
       0.0       0.25      0.523      0.822      1.131      1.458      1.802
2.166
     2.549      2.953      3.380      3.830      4.304      4.805      5.333
5.890
     6.478      7.098      7.752      8.442      9.170      9.938     10.747
11.601
    12.503     13.453     14.456     15.514     16.629     17.807     19.048
20.358
    21.740     23.198     24.735     26.357     28.068     29.873     31.776
33.784
    35.903     38.138     40.495     42.982     45.605     48.373     51.292
54.371
    57.619     61.046     64.660     68.473     72.495     76.738     81.214
85.935
    90.916     96.170    101.712    107.558    113.725    120.230    127.093
134.332
   141.969    150.024    158.522    167.485    176.941    186.916    197.438
208.538
   220.246    232.598    245.626    259.370    273.869    289.163    305.296
322.314
   340.267    359.205    379.182    400.255    422.485    445.934    470.671
496.765
   524.291    553.328    583.958    616.269    650.353    686.308    724.235
764.244
   806.449    850.970    897.934    947.476    1000.0
```

```
LAYER----1----*----2----*----3----*----4----*----5----*----6----*----7--
--*----8
    1
      10.0

ELEME ---   100  101    0    0   0.00000  1000.000
A1  1          GEYSR .1963E+010.3927E+00          0.1250E+00          -
.5000E+01
A1  2          GEYSR .6630E+010.1326E+01          0.3865E+00          -
.5000E+01
A1  3          GEYSR .1263E+020.2527E+01          0.6725E+00          -
.5000E+01
A1  4          GEYSR .1896E+020.3792E+01          0.9765E+00          -
.5000E+01
A1  5          GEYSR .2660E+020.5319E+01          0.1294E+01          -
.5000E+01
A1  6          GEYSR .3523E+020.7046E+01          0.1630E+01          -
.5000E+01
A1  7          GEYSR .4538E+020.9075E+01          0.1984E+01          -
.5000E+01
A1  8          GEYSR .5673E+020.1135E+02          0.2357E+01          -
.5000E+01
A1  9          GEYSR .6983E+020.1397E+02          0.2751E+01          -
.5000E+01
A1 10          GEYSR .8495E+020.1699E+02          0.3167E+01          -
.5000E+01
A1 11          GEYSR .1019E+030.2039E+02          0.3605E+01          -
.5000E+01
A1 12          GEYSR .1211E+030.2422E+02          0.4067E+01          -
.5000E+01
A1 13          GEYSR .1434E+030.2867E+02          0.4554E+01          -
.5000E+01
A1 14          GEYSR .1682E+030.3363E+02          0.5069E+01          -
.5000E+01
A1 15          GEYSR .1964E+030.3928E+02          0.5611E+01          -
.5000E+01
A1 16          GEYSR .2285E+030.4569E+02          0.6184E+01          -
.5000E+01
A1 17          GEYSR .2644E+030.5289E+02          0.6788E+01          -
.5000E+01
A1 18          GEYSR .3051E+030.6102E+02          0.7425E+01          -
.5000E+01
A1 19          GEYSR .3510E+030.7021E+02          0.8097E+01          -
.5000E+01
A1 20          GEYSR .4028E+030.8056E+02          0.8806E+01          -
.5000E+01
A1 21          GEYSR .4610E+030.9221E+02          0.9554E+01          -
.5000E+01
A1 22          GEYSR .5257E+030.1051E+03          0.1034E+02          -
.5000E+01
A1 23          GEYSR .5996E+030.1199E+03          0.1117E+02          -
.5000E+01
A1 24          GEYSR .6830E+030.1366E+03          0.1205E+02          -
.5000E+01
A1 25          GEYSR .7747E+030.1549E+03          0.1298E+02          -
.5000E+01
A1 26          GEYSR .8794E+030.1759E+03          0.1395E+02          -
.5000E+01
A1 27          GEYSR .9961E+030.1992E+03          0.1498E+02          -
.5000E+01
```

```
A1 28          GEYSR .1126E+040.2252E+03          0.1607E+02          -
.5000E+01
A1 29          GEYSR .1274E+040.2549E+03          0.1722E+02          -
.5000E+01
A1 30          GEYSR .1437E+040.2874E+03          0.1843E+02          -
.5000E+01
A1 31          GEYSR .1622E+040.3243E+03          0.1970E+02          -
.5000E+01
A1 32          GEYSR .1828E+040.3656E+03          0.2105E+02          -
.5000E+01
A1 33          GEYSR .2058E+040.4117E+03          0.2247E+02          -
.5000E+01
A1 34          GEYSR .2315E+040.4629E+03          0.2397E+02          -
.5000E+01
A1 35          GEYSR .2603E+040.5207E+03          0.2555E+02          -
.5000E+01
A1 36          GEYSR .2925E+040.5851E+03          0.2721E+02          -
.5000E+01
A1 37          GEYSR .3286E+040.6571E+03          0.2897E+02          -
.5000E+01
A1 38          GEYSR .3686E+040.7371E+03          0.3082E+02          -
.5000E+01
A1 39          GEYSR .4136E+040.8271E+03          0.3278E+02          -
.5000E+01
A1 40          GEYSR .4639E+040.9278E+03          0.3484E+02          -
.5000E+01
A1 41          GEYSR .5199E+040.1040E+04          0.3702E+02          -
.5000E+01
A1 42          GEYSR .5823E+040.1165E+04          0.3932E+02          -
.5000E+01
A1 43          GEYSR .6522E+040.1304E+04          0.4174E+02          -
.5000E+01
A1 44          GEYSR .7300E+040.1460E+04          0.4429E+02          -
.5000E+01
A1 45          GEYSR .8172E+040.1634E+04          0.4699E+02          -
.5000E+01
A1 46          GEYSR .9140E+040.1828E+04          0.4983E+02          -
.5000E+01
A1 47          GEYSR .1022E+050.2044E+04          0.5283E+02          -
.5000E+01
A1 48          GEYSR .1143E+050.2285E+04          0.5600E+02          -
.5000E+01
A1 49          GEYSR .1278E+050.2555E+04          0.5933E+02          -
.5000E+01
A1 50          GEYSR .1427E+050.2854E+04          0.6285E+02          -
.5000E+01
A1 51          GEYSR .1595E+050.3190E+04          0.6657E+02          -
.5000E+01
A1 52          GEYSR .1781E+050.3562E+04          0.7048E+02          -
.5000E+01
A1 53          GEYSR .1989E+050.3978E+04          0.7462E+02          -
.5000E+01
A1 54          GEYSR .2221E+050.4442E+04          0.7898E+02          -
.5000E+01
A1 55          GEYSR .2479E+050.4958E+04          0.8357E+02          -
.5000E+01
A1 56          GEYSR .2767E+050.5535E+04          0.8843E+02          -
.5000E+01
A1 57          GEYSR .3088E+050.6176E+04          0.9354E+02          -
.5000E+01
```

```
A1 58          GEYSR .3445E+050.6891E+04          0.9894E+02          -
.5000E+01
A1 59          GEYSR .3843E+050.7687E+04          0.1046E+03          -
.5000E+01
A1 60          GEYSR .4287E+050.8574E+04          0.1106E+03          -
.5000E+01
A1 61          GEYSR .4781E+050.9562E+04          0.1170E+03          -
.5000E+01
A1 62          GEYSR .5332E+050.1066E+05          0.1237E+03          -
.5000E+01
A1 63          GEYSR .5945E+050.1189E+05          0.1307E+03          -
.5000E+01
A1 64          GEYSR .6629E+050.1326E+05          0.1382E+03          -
.5000E+01
A1 65          GEYSR .7389E+050.1478E+05          0.1460E+03          -
.5000E+01
A1 66          GEYSR .8237E+050.1647E+05          0.1543E+03          -
.5000E+01
A1 67          GEYSR .9180E+050.1836E+05          0.1630E+03          -
.5000E+01
A1 68          GEYSR .1023E+060.2046E+05          0.1722E+03          -
.5000E+01
A1 69          GEYSR .1140E+060.2280E+05          0.1819E+03          -
.5000E+01
A1 70          GEYSR .1271E+060.2541E+05          0.1922E+03          -
.5000E+01
A1 71          GEYSR .1416E+060.2831E+05          0.2030E+03          -
.5000E+01
A1 72          GEYSR .1577E+060.3154E+05          0.2144E+03          -
.5000E+01
A1 73          GEYSR .1757E+060.3515E+05          0.2264E+03          -
.5000E+01
A1 74          GEYSR .1957E+060.3915E+05          0.2391E+03          -
.5000E+01
A1 75          GEYSR .2180E+060.4361E+05          0.2525E+03          -
.5000E+01
A1 76          GEYSR .2429E+060.4858E+05          0.2666E+03          -
.5000E+01
A1 77          GEYSR .2705E+060.5410E+05          0.2815E+03          -
.5000E+01
A1 78          GEYSR .3013E+060.6026E+05          0.2972E+03          -
.5000E+01
A1 79          GEYSR .3355E+060.6711E+05          0.3138E+03          -
.5000E+01
A1 80          GEYSR .3737E+060.7474E+05          0.3313E+03          -
.5000E+01
A1 81          GEYSR .4162E+060.8323E+05          0.3497E+03          -
.5000E+01
A1 82          GEYSR .4634E+060.9268E+05          0.3692E+03          -
.5000E+01
A1 83          GEYSR .5160E+060.1032E+06          0.3897E+03          -
.5000E+01
A1 84          GEYSR .5746E+060.1149E+06          0.4114E+03          -
.5000E+01
A1 85          GEYSR .6397E+060.1279E+06          0.4342E+03          -
.5000E+01
A1 86          GEYSR .7123E+060.1425E+06          0.4583E+03          -
.5000E+01
A1 87          GEYSR .7931E+060.1586E+06          0.4837E+03          -
.5000E+01
```

```
A1 88          GEYSR .8830E+060.1766E+06          0.5105E+03          -
.5000E+01
A1 89          GEYSR .9830E+060.1966E+06          0.5388E+03          -
.5000E+01
A1 90          GEYSR .1094E+070.2189E+06          0.5686E+03          -
.5000E+01
A1 91          GEYSR .1218E+070.2437E+06          0.6001E+03          -
.5000E+01
A1 92          GEYSR .1356E+070.2713E+06          0.6333E+03          -
.5000E+01
A1 93          GEYSR .1510E+070.3020E+06          0.6683E+03          -
.5000E+01
A1 94          GEYSR .1681E+070.3361E+06          0.7053E+03          -
.5000E+01
A1 95          GEYSR .1871E+070.3742E+06          0.7442E+03          -
.5000E+01
A1 96          GEYSR .2083E+070.4165E+06          0.7853E+03          -
.5000E+01
A1 97          GEYSR .2318E+070.4636E+06          0.8287E+03          -
.5000E+01
A1 98          GEYSR .2580E+070.5161E+06          0.8745E+03          -
.5000E+01
A1 99          GEYSR .2872E+070.5744E+06          0.9227E+03          -
.5000E+01
A11 0          GEYSR .3214E+070.6427E+06          0.9737E+03          -
.5000E+01

CONNE
A1  1A1  2                  10.1250E+000.1365E+000.1571E+02
A1  2A1  3                  10.1365E+000.1495E+000.3286E+02
A1  3A1  4                  10.1495E+000.1545E+000.5165E+02
A1  4A1  5                  10.1545E+000.1635E+000.7106E+02
A1  5A1  6                  10.1635E+000.1720E+000.9161E+02
A1  6A1  7                  10.1720E+000.1820E+000.1132E+03
A1  7A1  8                  10.1820E+000.1915E+000.1361E+03
A1  8A1  9                  10.1915E+000.2020E+000.1602E+03
A1  9A1 10                  10.2020E+000.2135E+000.1855E+03
A1 10A1 11                  10.2135E+000.2250E+000.2124E+03
A1 11A1 12                  10.2250E+000.2370E+000.2406E+03
A1 12A1 13                  10.2370E+000.2505E+000.2704E+03
A1 13A1 14                  10.2505E+000.2640E+000.3019E+03
A1 14A1 15                  10.2640E+000.2785E+000.3351E+03
A1 15A1 16                  10.2785E+000.2940E+000.3701E+03
A1 16A1 17                  10.2940E+000.3100E+000.4070E+03
A1 17A1 18                  10.3100E+000.3270E+000.4460E+03
A1 18A1 19                  10.3270E+000.3450E+000.4871E+03
A1 19A1 20                  10.3450E+000.3640E+000.5304E+03
A1 20A1 21                  10.3640E+000.3840E+000.5762E+03
A1 21A1 22                  10.3840E+000.4045E+000.6244E+03
A1 22A1 23                  10.4045E+000.4270E+000.6753E+03
A1 23A1 24                  10.4270E+000.4510E+000.7289E+03
A1 24A1 25                  10.4510E+000.4750E+000.7856E+03
A1 25A1 26                  10.4750E+000.5015E+000.8453E+03
A1 26A1 27                  10.5015E+000.5290E+000.9083E+03
A1 27A1 28                  10.5290E+000.5575E+000.9748E+03
A1 28A1 29                  10.5575E+000.5890E+000.1045E+04
A1 29A1 30                  10.5890E+000.6205E+000.1119E+04
A1 30A1 31                  10.6205E+000.6550E+000.1197E+04
A1 31A1 32                  10.6550E+000.6910E+000.1279E+04
A1 32A1 33                  10.6910E+000.7290E+000.1366E+04
A1 33A1 34                  10.7290E+000.7685E+000.1458E+04
```

```
A1 34A1 35                  10.7685E+000.8110E+000.1554E+04
A1 35A1 36                  10.8110E+000.8555E+000.1656E+04
A1 36A1 37                  10.8555E+000.9025E+000.1764E+04
A1 37A1 38                  10.9025E+000.9515E+000.1877E+04
A1 38A1 39                  10.9515E+000.1004E+010.1997E+04
A1 39A1 40                  10.1004E+010.1059E+010.2123E+04
A1 40A1 41                  10.1059E+010.1117E+010.2256E+04
A1 41A1 42                  10.1117E+010.1178E+010.2396E+04
A1 42A1 43                  10.1178E+010.1244E+010.2544E+04
A1 43A1 44                  10.1244E+010.1311E+010.2701E+04
A1 44A1 45                  10.1311E+010.1384E+010.2865E+04
A1 45A1 46                  10.1384E+010.1460E+010.3039E+04
A1 46A1 47                  10.1460E+010.1540E+010.3223E+04
A1 47A1 48                  10.1540E+010.1624E+010.3416E+04
A1 48A1 49                  10.1624E+010.1713E+010.3620E+04
A1 49A1 50                  10.1713E+010.1807E+010.3836E+04
A1 50A1 51                  10.1807E+010.1907E+010.4063E+04
A1 51A1 52                  10.1907E+010.2011E+010.4302E+04
A1 52A1 53                  10.2011E+010.2121E+010.4555E+04
A1 53A1 54                  10.2121E+010.2238E+010.4822E+04
A1 54A1 55                  10.2238E+010.2361E+010.5103E+04
A1 55A1 56                  10.2361E+010.2490E+010.5399E+04
A1 56A1 57                  10.2490E+010.2627E+010.5712E+04
A1 57A1 58                  10.2627E+010.2771E+010.6043E+04
A1 58A1 59                  10.2771E+010.2923E+010.6391E+04
A1 59A1 60                  10.2923E+010.3083E+010.6758E+04
A1 60A1 61                  10.3083E+010.3253E+010.7146E+04
A1 61A1 62                  10.3253E+010.3431E+010.7554E+04
A1 62A1 63                  10.3431E+010.3619E+010.7985E+04
A1 63A1 64                  10.3619E+010.3819E+010.8440E+04
A1 64A1 65                  10.3819E+010.4028E+010.8920E+04
A1 65A1 66                  10.4028E+010.4249E+010.9426E+04
A1 66A1 67                  10.4249E+010.4482E+010.9960E+04
A1 67A1 68                  10.4482E+010.4728E+010.1052E+05
A1 68A1 69                  10.4728E+010.4987E+010.1112E+05
A1 69A1 70                  10.4987E+010.5261E+010.1174E+05
A1 70A1 71                  10.5261E+010.5550E+010.1241E+05
A1 71A1 72                  10.5550E+010.5854E+010.1310E+05
A1 72A1 73                  10.5854E+010.6176E+010.1384E+05
A1 73A1 74                  10.6176E+010.6514E+010.1461E+05
A1 74A1 75                  10.6514E+010.6872E+010.1543E+05
A1 75A1 76                  10.6872E+010.7250E+010.1630E+05
A1 76A1 77                  10.7250E+010.7647E+010.1721E+05
A1 77A1 78                  10.7647E+010.8066E+010.1817E+05
A1 78A1 79                  10.8066E+010.8509E+010.1918E+05
A1 79A1 80                  10.8509E+010.8976E+010.2025E+05
A1 80A1 81                  10.8976E+010.9469E+010.2138E+05
A1 81A1 82                  10.9469E+010.9989E+010.2257E+05
A1 82A1 83                  10.9989E+010.1054E+020.2382E+05
A1 83A1 84                  10.1054E+020.1112E+020.2515E+05
A1 84A1 85                  10.1112E+020.1172E+020.2655E+05
A1 85A1 86                  10.1172E+020.1237E+020.2802E+05
A1 86A1 87                  10.1237E+020.1305E+020.2957E+05
A1 87A1 88                  10.1305E+020.1376E+020.3121E+05
A1 88A1 89                  10.1376E+020.1452E+020.3294E+05
A1 89A1 90                  10.1452E+020.1531E+020.3477E+05
A1 90A1 91                  10.1531E+020.1616E+020.3669E+05
A1 91A1 92                  10.1616E+020.1704E+020.3872E+05
A1 92A1 93                  10.1704E+020.1798E+020.4086E+05
A1 93A1 94                  10.1798E+020.1896E+020.4312E+05
A1 94A1 95                  10.1896E+020.2000E+020.4551E+05
```

```
A1 95A1 96                    10.2000E+020.2110E+020.4802E+05
A1 96A1 97                    10.2110E+020.2226E+020.5067E+05
A1 97A1 98                    10.2226E+020.2348E+020.5347E+05
A1 98A1 99                    10.2348E+020.2477E+020.5642E+05
A1 99A11 0                    10.2477E+020.2626E+020.5953E+05

GENER----1----*----2----*----3----*----4----*----5----*----6----*----7--
--*----8
A1  1                              DELV    1.0E-13  1378.6E3      10.0

ENDCY----1----*----2----*----3----*----4----*----5----*----6----*----7--
--*----8


#Linear RP / Leverett CP ITOUGH2 input file
> PARAMETERS
  >> ABSOLUTE permeability
     >>> MATERIAL: GEYSR
         >>>> LOGARITHM
         >>>> INDEX: 1
         >>>> DEVIATION: 0.2
         <<<<
     <<<

  >> RELATIVE permeability function
     >>> MATERIAL: GEYSR
         >>>> PARAMETER No.: 1
         >>>> ANNOTATION   : Slr (RP)
         >>>> standard DEVIATION : 0.05
         >>>> max STEP : 0.05
         >>>> PERTURB : -0.001
         >>>> estimate VALUE
         >>>> RANGE  : 0.00 0.50
         <<<<
     >>> MATERIAL: GEYSR
         >>>> PARAMETER No.: 2
         >>>> ANNOTATION   : Sgr
         >>>> standard DEVIATION : 0.05
         >>>> max STEP : 0.05
         >>>> PERTURB : -0.001
         >>>> estimate VALUE
         >>>> RANGE  : 0.00 0.50
         <<<<
     >>> MATERIAL: GEYSR
         >>>> PARAMETER No.: 3
         >>>> ANNOTATION   : Sls
         >>>> standard DEVIATION : 0.05
         >>>> max STEP : 0.05
         >>>> PERTURB : -0.001
         >>>> estimate VALUE
         >>>> RANGE  : 0.51 1.00
         <<<<
     >>> MATERIAL: GEYSR
         >>>> PARAMETER No.: 4
         >>>> ANNOTATION   : Sgs
         >>>> standard DEVIATION : 0.05
         >>>> max STEP : 0.02
         >>>> estimate VALUE
         >>>> RANGE  : 0.51 1.00
         >>>> PERTURB : -0.001
         <<<<
```

```
     <<<

  >> parameters of the CAPILLARY pressure function
     >>> MATERIAL: GEYSR
         >>>> PARAMETER No.:  1
         >>>> ANNOTATION  :  Po
         >>>> standard DEVIATION : 0.50
         >>>> max STEP: 0.2
         <<<<
     >>> MATERIAL: GEYSR
         >>>> PARAMETER No.: 2
         >>>> ANNOTATION   : Slr
         >>>> standard DEVIATION : 0.05
         >>>> max STEP : 0.05
         >>>> PERTURB : -0.001
         >>>> estimate VALUE
         >>>> RANGE  : 0.00 1.00
         <<<<
     <<<
  <<

> OBSERVATIONS
  >> : 100 EQUALLY spaced TIMES in SECONDS between
     1.0   1.0E10

  >> CHANGE in total MASS
     >>> entire MODEL
         >>>> ANNOTATION: Masscum
         <<<<
     <<<

  >> TEMPERATURE
     >>> ELEMENT: A1__1
         >>>> ANNOTATION: T1
         >>>> COLUMNS: 1 2
         >>>> PICK : 10
         >>>> NO DATA
         >>>> DEVIATION: 2.0 deg C
         <<<<

     >>> ELEMENT: A1_87
         >>>> ANNOTATION: T2
         >>>> COLUMNS: 1 3
         >>>> PICK : 10
         >>>> NO DATA
         >>>> DEVIATION: 1.0 deg C
         <<<<

     >>> ELEMENT: A11_0
         >>>> ANNOTATION: T3
         >>>> COLUMNS: 1 4
         >>>> PICK : 10
         >>>> NO DATA
         >>>> DEVIATION: 1.0 deg C
         <<<<
     <<<

  >> PRESSURE
     >>> ELEMENT: A1__1
         >>>> ANNOTATION: P1
```

```
        >>>> COLUMNS: 1 2
        >>>> FACTOR: 1E6
        >>>> PICK : 10
        >>>> NO DATA
        <<<<

    >>> ELEMENT: A1_87
        >>>> ANNOTATION: P2
        >>>> COLUMNS: 1 3
        >>>> FACTOR: 1E6
        >>>> PICK : 10
        >>>> NO DATA
        <<<<

    >>> ELEMENT: A11_0
        >>>> ANNOTATION: P3
        >>>> COLUMNS: 1 4
        >>>> FACTOR: 1E6
        >>>> PICK : 10
        >>>> NO DATA
        <<<<
    <<<

>> LIQUID SATURATION
    >>> ELEMENT: A1__1
        >>>> ANNOTATION: Sw1
        >>>> COLUMNS: 1 2
        >>>> NO DATA
        >>>> DEVIATION: 0.02
        <<<<

    >>> ELEMENT: A1_87
        >>>> ANNOTATION: Sw2
        >>>> COLUMNS: 1 3
        >>>> NO DATA
        >>>> DEVIATION: 0.01
        <<<<

    >>> ELEMENT: A11_0
        >>>> ANNOTATION: Sw3
        >>>> COLUMNS: 1 4
        >>>> NO DATA
        >>>> DEVIATION: 0.01
        <<<<

    <<<

>> VAPOR GENERATION

    >>> SINK: A1__1
        >>>> ANNOTATION: Steam
        >>>> NO DATA
        <<<<
    <<<

>> LIQUID GENERATION

    >>> SINK: A1__1
        >>>> ANNOTATION: Water
        >>>> NO DATA
        <<<<
```

```
      <<<
  >> ENTHALPY
      >>> SINK: A1__1
          >>>> ANNOTATION: Enthalpy
          >>>> FACTOR: 1000.0
          >>>> NO DATA
          <<<<
      <<<
  >> CUMULATIVE VAPOR
      >>> SINK: A1__1
          >>>> ANNOTATION: SteamCum
          >>>> NO DATA
          <<<<
      <<<
  >> CUMULATIVE LIQUID
      >>> SINK: A1__1
          >>>> ANNOTATION: WaterCum
          >>>> NO DATA
          <<<<
      <<<
  <<
> COMPUTATION
  >> STOPPING criteria
      >>> IGNORE WARNINGS
      >>> max. no. of ITERATIONS: 20
      >>> CONSECUTIVE: 100
      >>> INCOMPLETE: 20
      >>> LEVENBERG: 0.1
      >>> STEP : 1.0
      <<<
  >> JACOBIAN
      >>> FORWARD: 8
      >>> PERTURB: 0.01
      <<<
  >> OPTIONS
#     >>> QUADRATIC-LINEAR: 3.0
#     >>> perform a SENSITIVITY analysis
      >>> DIRECT
      <<<
  >> OUTPUT
      >>> PLOTFILE: COLUMNS
      >>> DAYS
      >>> generate file with CHARACTERISTIC curves
      <<<
  <<
<
#Linear RP / Leverett CP ITOUGH2 input file
> PARAMETERS
  >> ABSOLUTE permeability
      >>> MATERIAL: GEYSR
          >>>> LOGARITHM
          >>>> INDEX: 1
```

```
        >>>> DEVIATION: 0.2
        <<<<
    <<<

>> RELATIVE permeability function
    >>> MATERIAL: GEYSR
        >>>> PARAMETER No.: 1
        >>>> ANNOTATION   : Slr (RP)
        >>>> standard DEVIATION : 0.05
        >>>> max STEP : 0.05
        >>>> PERTURB : -0.001
        >>>> estimate VALUE
        >>>> RANGE  : 0.00 0.50
        <<<<
    >>> MATERIAL: GEYSR
        >>>> PARAMETER No.: 2
        >>>> ANNOTATION   : Sgr
        >>>> standard DEVIATION : 0.05
        >>>> max STEP : 0.05
        >>>> PERTURB : -0.001
        >>>> estimate VALUE
        >>>> RANGE  : 0.00 0.50
        <<<<
    >>> MATERIAL: GEYSR
        >>>> PARAMETER No.: 3
        >>>> ANNOTATION   : Sls
        >>>> standard DEVIATION : 0.05
        >>>> max STEP : 0.05
        >>>> PERTURB : -0.001
        >>>> estimate VALUE
        >>>> RANGE  : 0.51 1.00
        <<<<
    >>> MATERIAL: GEYSR
        >>>> PARAMETER No.: 4
        >>>> ANNOTATION   : Sgs
        >>>> standard DEVIATION : 0.05
        >>>> max STEP : 0.02
        >>>> estimate VALUE
        >>>> RANGE  : 0.51 1.00
        >>>> PERTURB : -0.001
        <<<<

    <<<

>> parameters of the CAPILLARY pressure function
    >>> MATERIAL: GEYSR
        >>>> PARAMETER No.:  1
        >>>> ANNOTATION  :  Po
        >>>> standard DEVIATION : 0.50
        >>>> max STEP: 0.2
        <<<<
    >>> MATERIAL: GEYSR
        >>>> PARAMETER No.: 2
        >>>> ANNOTATION   : Slr
        >>>> standard DEVIATION : 0.05
        >>>> max STEP : 0.05
        >>>> PERTURB : -0.001
        >>>> estimate VALUE
        >>>> RANGE  : 0.00 1.00
        <<<<
    <<<
```

```
  <<

> OBSERVATIONS
  >> : 100 EQUALLY spaced TIMES in SECONDS between
     1.0   1.0E10

  >> CHANGE in total MASS
     >>> entire MODEL
         >>>> ANNOTATION: Masscum
         <<<<
     <<<

  >> TEMPERATURE
     >>> ELEMENT: A1__1
         >>>> ANNOTATION: T1
         >>>> COLUMNS: 1 2
         >>>> PICK : 10
         >>>> NO DATA
         >>>> DEVIATION: 2.0 deg C
         <<<<

     >>> ELEMENT: A1_87
         >>>> ANNOTATION: T2
         >>>> COLUMNS: 1 3
         >>>> PICK : 10
         >>>> NO DATA
         >>>> DEVIATION: 1.0 deg C
         <<<<

     >>> ELEMENT: A11_0
         >>>> ANNOTATION: T3
         >>>> COLUMNS: 1 4
         >>>> PICK : 10
         >>>> NO DATA
         >>>> DEVIATION: 1.0 deg C
         <<<<
     <<<

  >> PRESSURE
     >>> ELEMENT: A1__1
         >>>> ANNOTATION: P1
         >>>> COLUMNS: 1 2
         >>>> FACTOR: 1E6
         >>>> PICK : 10
         >>>> NO DATA
         <<<<

     >>> ELEMENT: A1_87
         >>>> ANNOTATION: P2
         >>>> COLUMNS: 1 3
         >>>> FACTOR: 1E6
         >>>> PICK : 10
         >>>> NO DATA
         <<<<

     >>> ELEMENT: A11_0
         >>>> ANNOTATION: P3
         >>>> COLUMNS: 1 4
         >>>> FACTOR: 1E6
         >>>> PICK : 10
         >>>> NO DATA
```

```
        <<<<
    <<<

>> LIQUID SATURATION
    >>> ELEMENT: A1__1
        >>>> ANNOTATION: Sw1
        >>>> COLUMNS: 1 2
        >>>> NO DATA
        >>>> DEVIATION: 0.02
        <<<<

    >>> ELEMENT: A1_87
        >>>> ANNOTATION: Sw2
        >>>> COLUMNS: 1 3
        >>>> NO DATA
        >>>> DEVIATION: 0.01
        <<<<

    >>> ELEMENT: A11_0
        >>>> ANNOTATION: Sw3
        >>>> COLUMNS: 1 4
        >>>> NO DATA
        >>>> DEVIATION: 0.01
        <<<<

    <<<

>> VAPOR GENERATION

    >>> SINK: A1__1
        >>>> ANNOTATION: Steam
        >>>> NO DATA
        <<<<
    <<<

>> LIQUID GENERATION

    >>> SINK: A1__1
        >>>> ANNOTATION: Water
        >>>> NO DATA
        <<<<
    <<<

>> ENTHALPY

    >>> SINK: A1__1
        >>>> ANNOTATION: Enthalpy
        >>>> FACTOR: 1000.0
        >>>> NO DATA
        <<<<
    <<<

>> CUMULATIVE VAPOR

    >>> SINK: A1__1
        >>>> ANNOTATION: SteamCum
        >>>> NO DATA
        <<<<
    <<<
```

```
  >> CUMULATIVE LIQUID

     >>> SINK: A1__1
         >>>> ANNOTATION: WaterCum
         >>>> NO DATA
         <<<<
     <<<

  <<

> COMPUTATION
  >> STOPPING criteria
     >>> IGNORE WARNINGS
     >>> max. no. of ITERATIONS: 20
     >>> CONSECUTIVE: 100
     >>> INCOMPLETE: 20
     >>> LEVENBERG: 0.1
     >>> STEP : 1.0
     <<<
  >> JACOBIAN
     >>> FORWARD: 8
     >>> PERTURB: 0.01
     <<<
  >> OPTIONS
#    >>> QUADRATIC-LINEAR: 3.0
#    >>> perform a SENSITIVITY analysis
     >>> DIRECT
     <<<
  >> OUTPUT
     >>> PLOTFILE: COLUMNS
     >>> DAYS
     >>> generate file with CHARACTERISTIC curves
     <<<
  <<
<
```